



Article

Design, Synthesis and Biological Evaluation of Novel 1,3,5-Triazines: Effect of Aromatic Ring Decoration on Affinity to 5-HT₇ Receptor

Damian Kułaga ^{1,*}, Anna Karolina Drabczyk ¹, Grzegorz Satała ², Gniewomir Latacz ³, Anna Boguszewska-Czubarą ⁴, Damian Płażuk ⁵ and Jolanta Jaśkowska ¹

¹ Department of Organic Chemistry and Technology, Faculty of Chemical Engineering and Technology, Cracow University of Technology, ul. Warszawska 24, 31-155 Kraków, Poland

² Department of Medicinal Chemistry, Maj Institute of Pharmacology, Polish Academy of Sciences, ul. Smętna 12, 31-343 Kraków, Poland

³ Department of Technology and Biotechnology of Drugs, Jagiellonian University Medical College, ul. Medyczna 9, 30-688 Kraków, Poland

⁴ Department of Medical Chemistry, Medical University of Lublin, ul. Chodźki 4a, 20-093 Lublin, Poland

⁵ Laboratory of Molecular Spectroscopy, Department of Organic Chemistry, Faculty of Chemistry, University of Lodz, ul. Tamka 12, 91-403 Łódź, Poland

* Correspondence: damian.kulaga@pk.edu.pl

Abstract: Considering the key functions of the 5-HT₇ receptor, especially in psychiatry, and the fact that effective and selective 5-HT₇ receptor ligands are yet to be available, in this work, we designed and synthesized novel 1,3,5-triazine derivatives particularly based on the evaluation of the effect of substituents at aromatic rings on biological activity. The tested compounds showed high affinity to the 5-HT₇ receptor, particularly ligands N²-(2-(5-fluoro-1H-indol-3-yl)ethyl)-N⁴-phenethyl-1,3,5-triazine-2,4,6-triamine **2** (K_i = 8 nM) and N²-(2-(1H-indol-3-yl)ethyl)-N⁴-(2-((4-fluorophenyl)amino)ethyl)-1,3,5-triazine-2,4,6-triamine **12** (K_i = 18 nM) which showed moderate metabolic stability, and affinity to the CYP3A4 isoenzyme. As for the hepatotoxicity evaluation, the tested compounds showed moderate cytotoxicity only at concentrations above 50 μM. Compound **12** exhibited less cardiotoxic effect than **2** on Danio rerio in vivo model.

Keywords: serotonin; microwave synthesis; CNS



Citation: Kułaga, D.; Drabczyk, A.K.; Satała, G.; Latacz, G.; Boguszewska-Czubarą, A.; Płażuk, D.; Jaśkowska, J. Design, Synthesis and Biological Evaluation of Novel 1,3,5-Triazines: Effect of Aromatic Ring Decoration on Affinity to 5-HT₇ Receptor. *Int. J. Mol. Sci.* **2022**, *23*, 13308. <https://doi.org/10.3390/ijms232113308>

Academic Editor: Alessandro Cannavo

Received: 4 October 2022

Accepted: 26 October 2022

Published: 1 November 2022

Publisher's Note: MDPI stays neutral with regard to jurisdictional claims in published maps and institutional affiliations.



Copyright: © 2022 by the authors. Licensee MDPI, Basel, Switzerland. This article is an open access article distributed under the terms and conditions of the Creative Commons Attribution (CC BY) license (<https://creativecommons.org/licenses/by/4.0/>).

1. Introduction

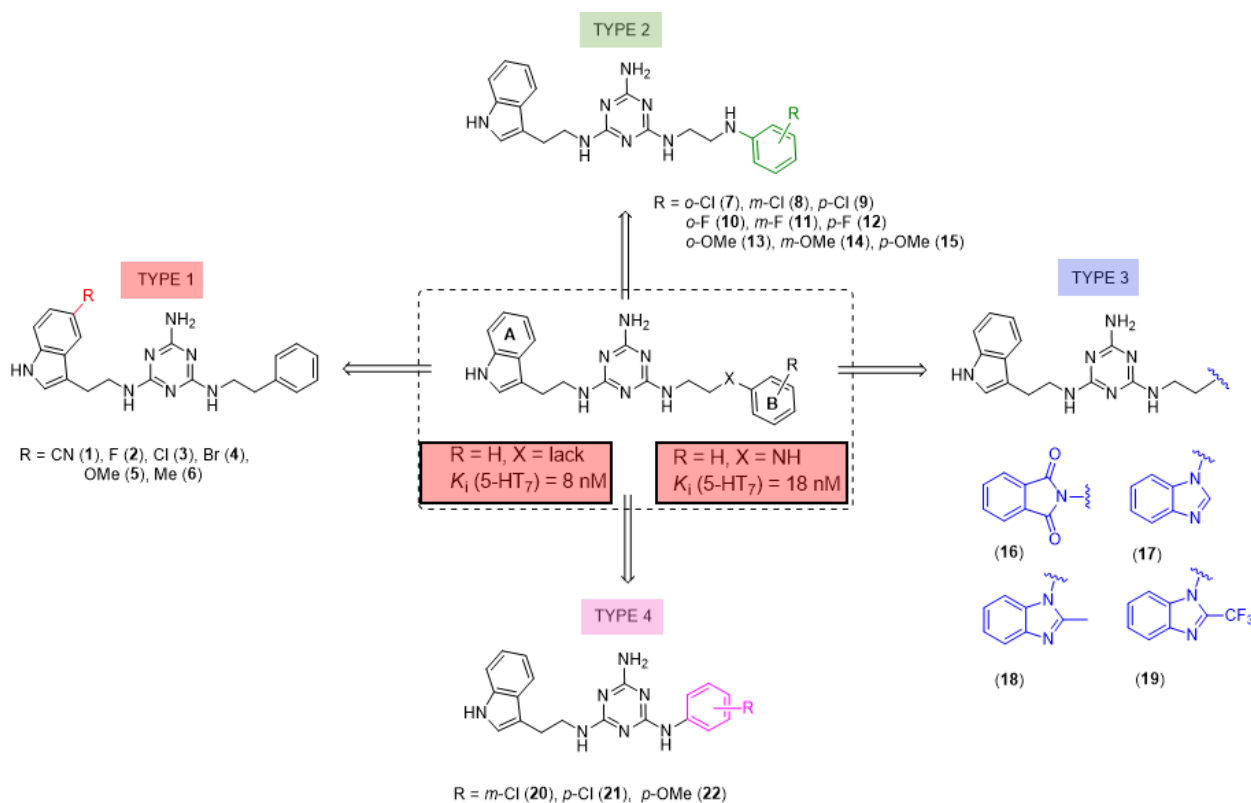
The 5-HT₇ receptor (5-HT₇R) is one of seven types of protein G-coupled aminergic serotonin receptors [1]. It is found in the central nervous system, mainly in the brain, in which it has regulatory functions, for example (the day–night cycle), and may affect behavior, mood, emotions, or memory [2,3]. The receptor is also expressed outside the central nervous system, e.g., in the intestines [4], mammary glands [5], lungs [6], or prostate [7].

Three human splicing variants (h5-HT_{7(a)}, h5HT_{7(b)}, and h5-HT_{7(d)}) have been reported so far. As long as the h5-HT_{7(a)} and h5-HT_{7(b)} variants do not differ significantly in terms of the number of amino acids in the C-terminal tail, for example, and maintain similar pharmacological properties, the h5-HT_{7(d)} variant shows the greatest differences in the C-terminal tail, which may lead to slightly different functionality [1]. The primary signaling pathway for the 5-HT₇ receptor involves the receptor binding the ligand, followed by phosphorylation of subunit G combined with its dissociation into subunit G_S and heterodimer G₁₂. In the subsequent stage, protein G_S (canonical signaling) is activated, which triggers isoform CA (adenyl cyclase) and leads to an intrinsic increase in cAMP (cyclic adenosine monophosphate) levels. cAMP induces PKA (protein kinase A) expression, which in turn induces further phosphorylation of other proteins, for example, on Ras, ERK, and Akt pathways. It has also been shown that protein G_S and protein G₁₂ (non-canonical

signaling) are activated by 5-HT₇R, which leads to further signaling in the cell and results in neurite outgrowth, synaptogenesis, and neuronal excitability [8,9].

It is well-known that 5-HT₇R is a binding site for several bioactive compounds with antidepressive or anxiolytic effects [2,3]. However, as the ligand–receptor complex may indirectly affect downstream signalization, 5-HT₇ receptor ligands may affect the expression of respective kinases or proteins (whose overexpression occurs in tumor cells). It is owing to this property, among other things, that some 5-HT₇ receptor antagonists or agonists have anticancer [10–12] or anti-inflammatory effects [13,14]. Based on the significant functions of 5-HT₇R and also the therapeutic effects that can be achieved owing to this receptor, it is justified to discover novel, selective and safe ligands of the receptor.

We recently proved that it was possible to forgo the well-known arylpiperazine pharmacophore while maintaining activity and selectivity toward 5-HT₇R [15]. The lead motif in the studies so far was an unsubstituted tryptamine core connected to aminotriazine. However, literature reports are available in which the incorporation of substituents at the indole C-5 position resulted in increased affinity toward 5-HT₇R. A particular effect was noted, with substituents being electron withdrawal groups (EWGs) [16,17]. Therefore, we decided in this report to synthesize a group of compounds 1–6 (Scheme 1, type 1) with a substituted indole C-5 position (by EWGs and EDGs (electron donating groups)) and subsequently to evaluate their effect on affinity toward the 5-HT₇ receptor. Another argument for synthesizing indole derivatives is the effect of heteroatoms on ADME-T parameters, particularly the fluorine atom [18,19]. We showed [20] that the compounds tested without any ring substituent (Figure 1A) had low in vitro metabolic stability. By incorporating chlorine in the structure [15] (Figure 1B), metabolic stability increased with a slight decrease in cytotoxicity in the HepG2 cell line. This correlation is also confirmed by the original report by Mattson et al. [21], in which the incorporation of fluorine atoms in the molecule increased stability almost five times compared to the unsubstituted compound (Figure 2).



Scheme 1. Structures of 2,4,6-triamino-1,3,5-triazine derivatives studied herein.

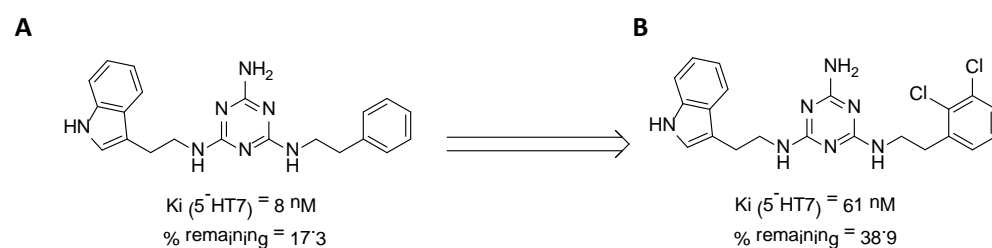


Figure 1. Effect of the chlorine atom on in vitro metabolic stability—two additional chlorine atoms (**B**) increase metabolic stability versus unsubstituted compound (**A**). % remaining: quantity of the compound that remained after incubation with mouse liver microsomes (MLMs) [15].

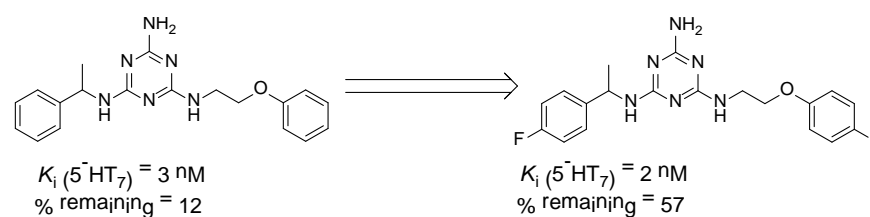


Figure 2. Effect of the fluorine atom on metabolic stability. % remaining: quantity of the compound that remained after incubation with human liver microsomes (HLMs) [21].

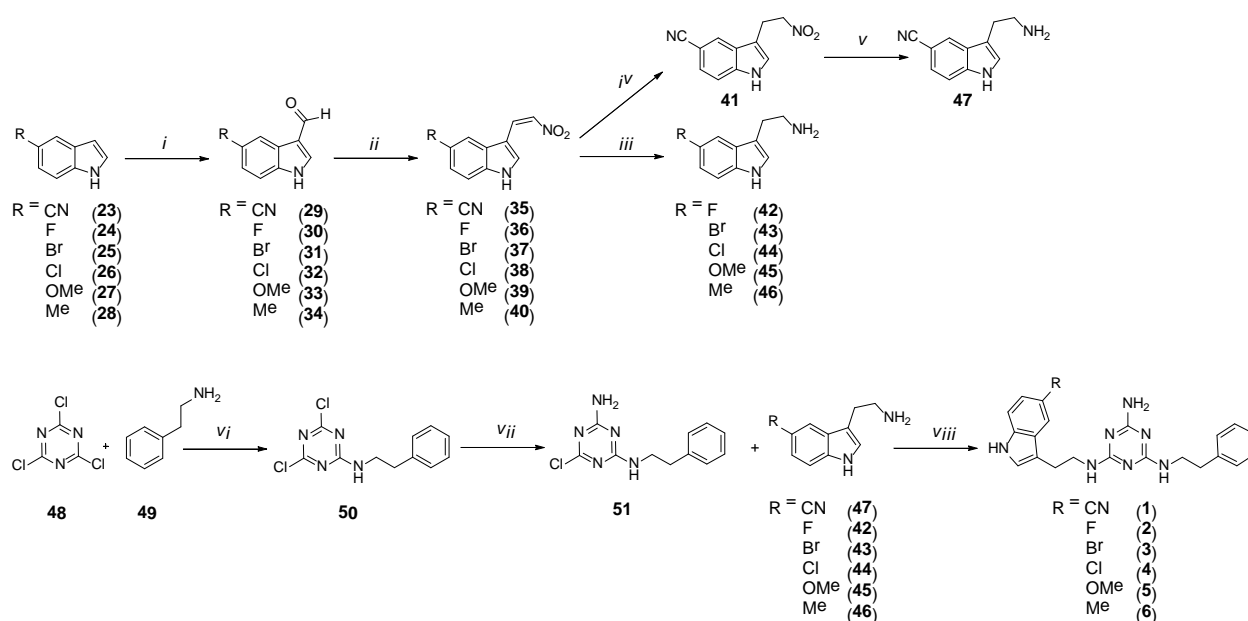
In our previous paper [15], we also investigated the effect of substituents (*ortho*-OMe and 2,3-Cl₂) at the phenyl ring attached to the aminoethyl chain on affinity toward 5-HT₇R. The substituents were found to reduce receptor affinity, but the effect of a specific substituent position on activity was not tested. To investigate this aspect, we decided to synthesize a group of ligands 7–15 (Scheme 1, type 2) containing Cl, F, and OMe at positions *ortho*-, *meta*-, and *para*- and to evaluate their effects on affinity toward 5-HT₇R. We also decided to incorporate more complex substituents into the structures of studied compounds (phthalimide **16** and benzimidazole **17–19** cores, Scheme 1, type 3) due to the potential formation of hydrogen bonds to stabilize the ligand–receptor additionally. Unexpectedly, we prepared compounds **20–22** without the aminoethyl chain in our synthesis experiments (Scheme 1, type 4). To determine the effect of the lack of an alkyl linker between the triazine and the aromatic system on affinity to the receptors in question, we also evaluated these compounds in in vitro tests. All the resulting compounds were tested in an extended receptor panel, including affinity toward 5-HT_{1A}, 5-HT_{2A}, 5-HT₆, and D₂ receptors, to determine the selectivity of the compounds. Bioconformation and key interactions involved in the forming the ligand–receptor complex were proposed for active structures. The two best compounds were evaluated in terms of safety and bioavailability in in vitro ADME-Tox tests.

2. Results

2.1. Chemistry

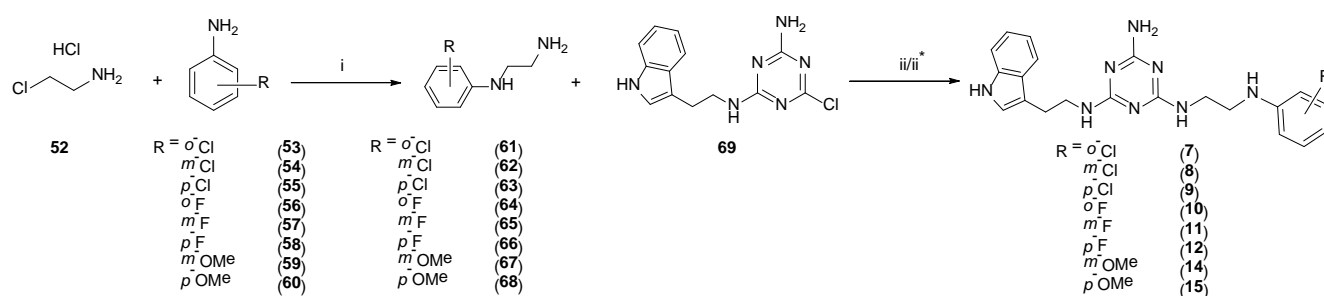
Final type 1 compounds were synthesized according to Scheme 2, starting from commercially available 5-substituted indoles **23–28**, converted to 3-substituted aldehydes **29–34** via Vilsmeier-Haack formylation with 90–100% yields. In a subsequent stage, the aldehydes were subjected to the Henry reaction to obtain nitrovinyl derivatives **35–40**. The synthesis of the derivatives initially followed patent [22] under conventional reflux of the reaction mixture. As long as yields of more than 90% were obtained in a small scale of 0.5–1 g, side products formed in the reaction mixture (according to TLC) with low yields of 40–56% when the scale was increased to 5 g. However, we found that performing the reactions under microwave irradiation ($P = 85 \text{ W}$) for 20 min allows obtaining desired products in more than 90% yields, irrespective of the scale. Crude **35–40** were used in the next stage without any further purification. As for compound **35**, another two stages involved reduction: first of the double bond using a mild reducing agent (NaBH_4) to give **41** and subsequently

reduction of the nitro group with zinc in boiling 36% HCl solution, to finally give compound **47**. As compounds **36–40** lacked the nitrile substituent, which could also be reduced in harsher conditions, simultaneous reduction of the double bond and the nitro group could be performed in the presence of LiAlH_4 to give final 5-substituted tryptamines **42–46**, respectively. The subsequent stage was the synthesis of core compounds **51**. Cyanuric chloride **48** was reacted with phenylethylamine **49** at 0°C , and the resulting product **50** was treated with ammonia water. Synthesis was conducted at room temperature for 5 h, and core compound **51** was obtained in 86% yield, which further reacted with 5-substituted tryptamines **42–47** to give final type 1 products with a yield of more than 50%. The synthesis of compounds **1–6** was conducted under microwave irradiation, similar to our previous reports [15].

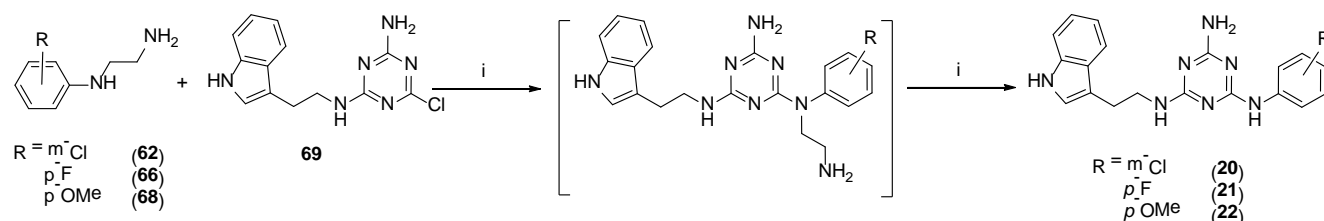


Scheme 2. Synthesis pathway for compounds of type 1 **1–6**. *i*—DMF, POCl_3 , 0°C then rt., 1 h; *ii*—ammonia acetate, nitromethane, MW, 20 min; *iii*— LiAlH_4 , THF, rt, 3 days; *iv*— NaBH_4 , MeOH/DMF, rt, 3 h; *v*—Zn, HCl, reflux, 5 h; *vi*—DIPEA, THF, 0°C , 2 h; *vii*—ammonia solution 20%, rt, 5 h; *viii*— K_2CO_3 , TBAB, DMF, MW, 2.5 min.

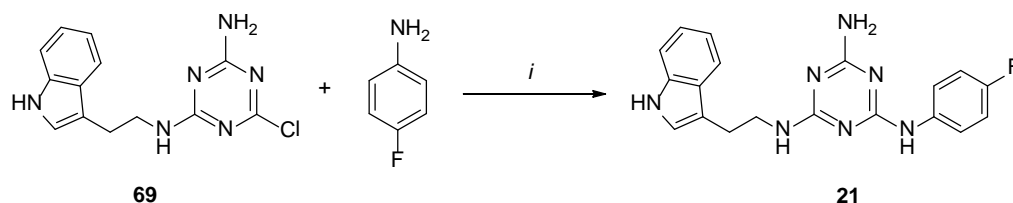
Type 2 compounds were synthesized according to Scheme 3. First, amines **61–68** were obtained in the reaction of 2-chloroethylamine hydrochloride **52** and appropriately substituted aniline **53–60**. Subsequently, the resulting compounds reacted with readily available [20] core compound **69** in the presence of K_2CO_3 and microwave irradiation ($p = 50\text{ W}$) for 2.5 min [15]. Final type 2 compounds were isolated with yields of 43–75%. In spite of the complete conversion of substrate **69** (according to TLC), compounds **8**, **12**, and **15** were not obtained. However, it was found that the ethyl bridge was probably eliminated during the reaction (see the mass spectra, Supplementary Materials) to give compounds **20–22** (Scheme 1, type 4) in which aniline derivatives were attached directly to the triazine system (Scheme 4). The resulting products were easily isolated during work-up as white precipitates, which did not require purification. Their structures were confirmed using spectroscopy: ^1H NMR, ^{13}C NMR, and MS. To confirm our hypothesis, we decided to synthesize the selected compound **21** starting from intermediate **69** and *para*-fluoroaniline (Scheme 5). The reaction was conducted similarly to the previous one in the presence of potassium carbonate (3 eq.) and sodium carbonate (3 eq.) to give title compound **21**. According to HPLC-MS analysis, the content of the desired product in the reaction mixture was 23% for potassium carbonate and 73% for sodium carbonate (see Supplementary Materials). Desired compounds **8**, **12**, and **15** were obtained with a yield of more or equal to 60% using the same synthesis method while only changing the base to sodium carbonate.



Scheme 3. Synthesis pathway for compounds of type 2, 7, 9–11, and 14. *i*–toluene, reflux, 20 h; *ii*– K_2CO_3 , TBAB, DMF, MW, 2.5 min; *ii** (for 8, 12, 15)– Na_2CO_3 , TBAB, DMF, MW, 2.5 min.

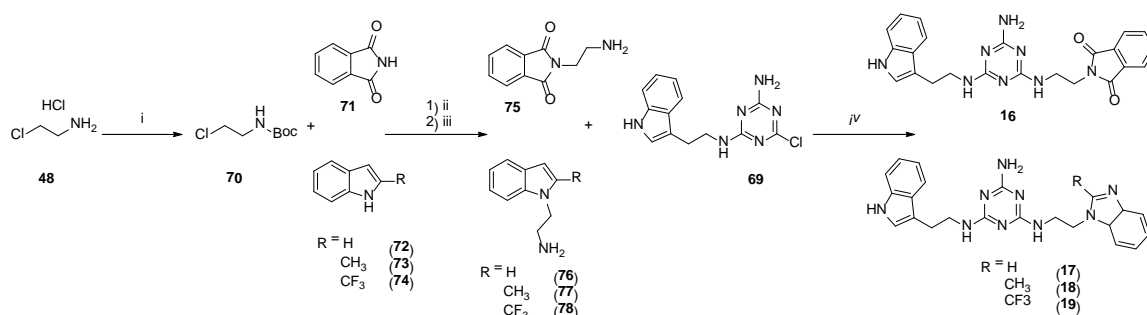


Scheme 4. Proposed synthesis pathway for compounds of type 4, 20–21. *i*– K_2CO_3 , TBAB, DMF, MW, 2.5 min.



Scheme 5. Synthesis of 21 in alternative pathway. *i*–base, TBAB, DMF, MW, 2.5 min.

The synthesis of type 3 compounds (Scheme 6) started with protecting 2-chloroethylamine hydrochloride **52** with a Boc group, followed by coupling of the resulting product **70** with phthalimide **71** or benzimidazole **72** and its derivatives **73** and **74**. The reactions were performed under microwave irradiation ($P = 60$ W) for 60 s in the presence of sodium hydroxide and TBAB (tetrabutylammonium bromide). Isolated products **75**–**78** reacted with **69** under microwave irradiation ($P = 50$ W) in the presence of K_2CO_3 and TBAB to give final compounds **15**–**18** with yields of 25–56%.



Scheme 6. Synthesis pathway for compounds of type 3, 16–19. *i*– Boc_2O , Et_2N , DCM, 0°C then rt, 12 h; *ii*– NaOH , TBAB, DMF, MW, 60 s; *iii*– 3N HCl in dioxane, DCM, rt, 12 h; *iv*– K_2CO_3 , TBAB, DMF, MW, 2.5 min.

2.2. Radioligand Binding and SAR

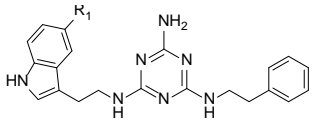
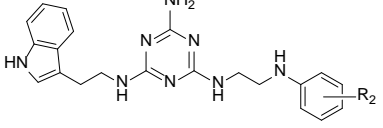
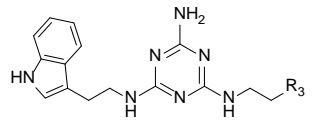
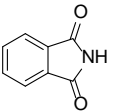
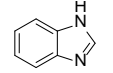
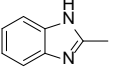
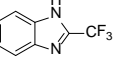
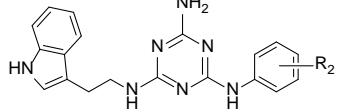
The affinity of the studied compounds to 5-HT_{1A}, 5-HT_{2A}, 5-HT₆, 5-HT₇, and D₂ receptors was evaluated by a radioligand assay, as reported previously (Table 1) [17]. Each compound was tested in triplicate at seven concentrations (from 0.1 nM to 100 μM). Inhibition constants (K_i) were calculated from the Cheng–Prusoff equation [23].

The substituent at indole position 5 in the A ring (type 1 compound) had no significant effect on increased binding to the 5-HT₇ receptor. The ligand with a weakly deactivating fluorine substituent **2** was found to be the most active among the tested type 1 compounds and showed an affinity of $K_i = 8$ nM toward 5-HT₇R. In addition, in terms of the effect of the halogen atom, ligand **3** with bromine (5-HT₇R $K_i = 126$ nM) had moderate activity, followed by ligand **4** with chlorine (5-HT₇R, $K_i = 481$ nM). Indole substitution at position 5 with CN, a strongly deactivating substituent (compound **1**), resulted in activity toward the 5-HT₇ receptor being lost. As for two activating substituents: Me (weakly activating) and OMe (strongly activating), moderate activity toward the 5-HT₇ receptor was shown for ligand **6** ($K_i = 100$ nM), while ligand **5** had a low activity with $K_i = 629$ nM. As for type 1 compounds, a halogen substituent at the B ring resulted in active (**9**, **11**, **12**) or moderately active ligands (**7**, **8**, **10**) with respect to 5-HT₇R, while a slightly larger substituent (OMe) resulted in the loss of activity. When analyzing the effect of the substituted position, ligands in the *para* position had the highest activity, and the *ortho* position was the least active. It is concluded based on analysis of the data that the fluorine substituent (*para* > *meta* > *ortho*) is the strongest, followed by chlorine (*para* > *meta* > *ortho*) and finally methoxy (*para* > *meta* > *ortho*). For example, *para*-F (**18**) and *para*-Cl (**9**), with K_i values of 18 nM and 19 nM, respectively, were found to be the most active ligands. Isomeric *meta*-F (**11**) and *meta*-Cl (**8**) compounds had slightly lower activity compared to the previous ones, with K_i values of 24 nM and 131 nM, respectively. Even though the compounds with the OMe substituent were inactive, a tendency for a relatively stronger *para* position compared to the weaker *meta* and, finally, the weakest *ortho* position was also seen in this group. As for type 3 ligands, incorporation of larger substituents R_3 resulted in most cases in the loss of activity ($K_i > 1000$ nM) toward 5-HT₇R (ligands **16**, **18**, and **19**). Only the ligand with an unsubstituted benzimidazole ring (**17**) had a moderate activity with $K_i = 227$ nM. The type 4 compounds are also found to be inactive (**20**, **21**) or weakly active (**22**), but they provide further evidence of the significant effect of the linker between the triazine core and the aromatic system [20]. When analyzing affinity to the other receptors tested (5-HT_{1A}, 5-HT_{2A}, 5-HT₆, and D₂), most of the designed compounds have no activity ($K_i > 1000$ nM) or low activity (500 nM < K_i < 1000 nM).

2.3. Atlas Activity Analysis: 3D-SAR

To better understand SAR, we determined specific activity maps as a function of shape, hydrophobicity, and electrostatics using Activity Atlas (Flare, Cresset) [24]. According to the ligand shape, the incorporation of large substituents at indole position 5 (A ring) results in reduced activity toward 5-HT₇R. A similar effect is found for substituents at the alkyaromatic ring (B ring). It can be concluded based on Figure 3B,D that large substituents (ligands **13–19**, $K_i > 226$ nM) cannot be accommodated in the receptor binding pocket, resulting in the loss of activity as shown by an increased number of steric clashes found between the ligand and the binding pocket. Ligands **7–12** with small substituents such as chlorine or fluorine show a much better fit to the binding pocket (lower number of steric clashes) as shown by their high or moderate activity to the 5-HT₇ receptor (Figure 3A,C). It is noted that no steric clashes were found between the substituent and the receptor binding pocket for the most active type 2 ligand **12** ($K_i = 18$ nM). This is due to the fact that ligands at the *para* positions are most preferred with the best fit to the receptor.

Table 1. Affinity (K_i in [nM]) and SD of the novel derivatives containing triazine motifs to 5-HT_{1A}R and D₂R.

Type No.	Ligand No.	R ₁	R ₂	R ₃	5-HT _{1A} R	5-HT _{2A} R	5-HT ₆ R	5-HT ₇ R	D ₂ R
	1	CN	-	-	12,980 ± 2354	927 ± 927	1563 ± 1563	2883 ± 351	-
	2	F	-	-	13,900 ± 1759	413 ± 67	505 ± 61	8 ± 2	-
	3	Br	-	-	10,950 ± 1598	942 ± 112	234 ± 27	126 ± 17	-
	4	Cl	-	-	3913 ± 581	559 ± 41	702 ± 48	481 ± 23	14,530 ± 2697
	5	OMe	-	-	3128 ± 758	883 ± 108	509 ± 33	629 ± 148	-
	6	Me	-	-	16,560 ± 1943	835 ± 168	714 ± 112	100 ± 15	-
	7	-	<i>o</i> -Cl	-	30,830 ± 4238	2125 ± 352	892 ± 144	423 ± 37	4294 ± 1028
	8	-	<i>m</i> -Cl	-	15,630 ± 1927	1800 ± 264	4022 ± 719	131 ± 16	1238 ± 257
	9	-	<i>p</i> -Cl	-	16,160 ± 2566	2698 ± 581	641 ± 84	19 ± 4	-
	10	-	<i>o</i> -F	-	36,510 ± 8652	1514 ± 362	982 ± 115	132 ± 9	20,410 ± 3695
	11	-	<i>m</i> -F	-	34,580 ± 5581	1277 ± 168	979 ± 237	24 ± 5	13,760 ± 2491
	12	-	<i>p</i> -F	-	43,250 ± 9541	3570 ± 491	1630 ± 301	18 ± 3	2999 ± 679
	13 *	-	<i>o</i> -OMe	-	37,040	14,390	2798	5823	3907
	14	-	<i>m</i> -OMe	-	108,900 ± 18,654	2449 ± 273	2790 ± 342	1036 ± 81	35,960 ± 8432
	15	-	<i>p</i> -OMe	-	-	-	-	756 ± 107	-
		16	-	-		138,800 ± 31,821	22,350 ± 3546	8760 ± 1762	21,560 ± 5127
17		-	-		63,010 ± 13,591	11,150 ± 2571	2629 ± 427	227 ± 37	-
18		-	-		180,200 ± 41,983	9355 ± 831	1958 ± 269	4128 ± 725	-
19		-	-		76,200 ± 18,615	4035 ± 537	825 ± 72	3464 ± 284	-
	20	-	<i>m</i> -Cl	-	14,100 ± 2594	2690 ± 549	2226 ± 528	1952 ± 261	2267 ± 153
	21	-	<i>p</i> -F	-	249,500 ± 54,268	884 ± 73	1765 ± 243	2052 ± 419	7033 ± 439
	22	-	<i>p</i> -OMe	-	79,830 ± 16,252	3110 ± 438	3742 ± 539	727 ± 107	-

Each compound was tested in triplicate at 7 concentrations (from 0.1 nM to 100 μM). Inhibition constants (K_i) were calculated from the Cheng–Prusoff equation [23]. Results were expressed as means of at least two separate experiments ± standard deviation (SD), *-according to ref. no [15].

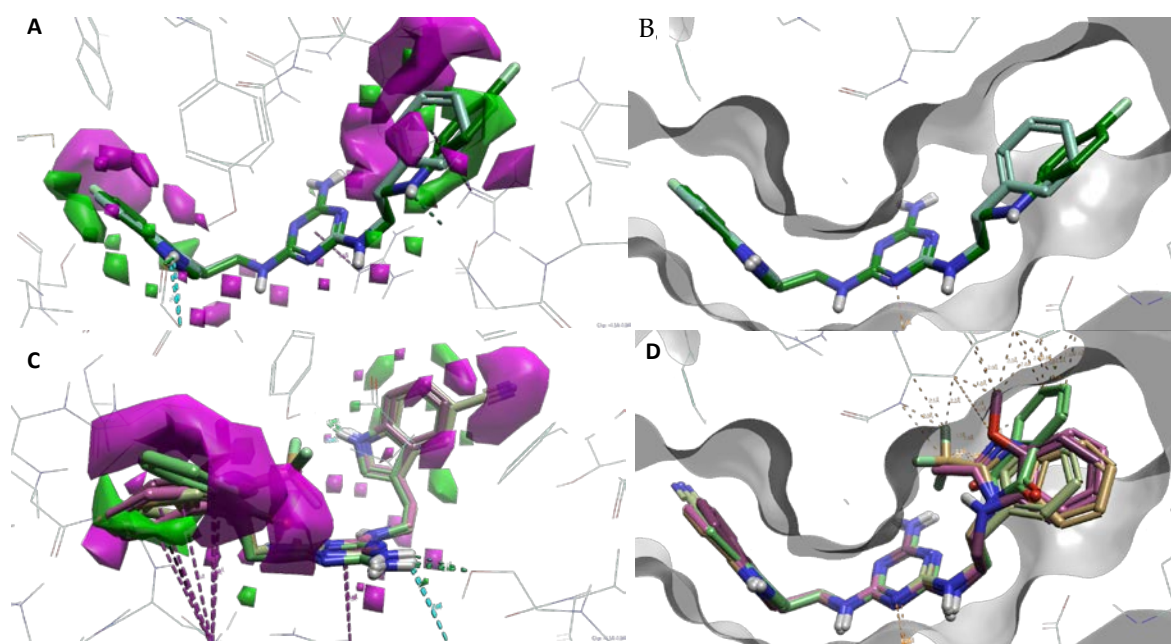


Figure 3. (A,B)—activity cliff summary maps as function of shape. (A)—map showing representative ligands **2** (teal) and **12** (green). Magenta represents unfavorable shape (more steric bulk leads to lower activity), and green represents favorable shape (more steric bulk leads to higher activity). (B)—map showing representative inactive ligands **16** (light brown), **18** (pink), and **19** (light green). (C,D)—binding side surface and sterically clashes (marked in dotted orange lines). (C)—representative active ligands **2** and **12**. (D)—representative inactive ligands **16**, **18**, and **19**. Magenta dotted lines represent π - π interactions, while turquoise and green represent hydrogen bonds with appropriate amino acids.

According to ligand hydrophobicity, type 2 ligands (ligands 7–12) show the best fit to the favorable hydrophobic region (squared green) due to the presence of a hydrophobic aromatic ring which may contribute to π - π interactions (B ring, Figure 4A). The unfavorable hydrophobic region (squared magenta) is not occupied by hydrophobic substituents. Type 3 ligands (ligands 16–19) are a different case. The favorable hydrophobic region is occupied by hydrophilic parts of the substituents (imide and imidazole systems), while the unfavorable hydrophobic region is occupied by the hydrophobic aromatic ring (Figure 4B). The effect of the hydrophobic/hydrophilic properties of substituents at indole position 5 (A ring) for type 1 ligands was difficult to determine based on our studies.

2.4. Molecular Modelling

The highly active compounds (**2** $K_i = 8$ nM and **12** $K_i = 18$ nM) were selected for studying their bioconformation and binding modes through molecular modeling using Induced Fit Docking (Schrodinger, Maestro [25]) followed by ligand–receptor complex optimization using a QM-MM mixed quantum mechanical method (Schrodinger, Maestro [25]) [15,20]. Both ligands occupy a binding pocket typical of 5-HT₇ receptor ligands [26]. They are oriented toward the inside of the receptor (between TMh3 and TMh5, TMh–*transmembrane helix*) with the tryptamine part, while the alkylaromatic part faces the external receptor surface (between TMh2 and TMh6). Both ligands have more linear bioconformation (Figure 5) with a clear bend of the alkylaromatic moiety and almost completely overlapping hydrogen bonds with the following amino acids: Glu366 (E7.34), Asp162 (D3.32), Ile233, Ser243 (S5.42) (for ligand **2**), and π - π stacking hydrophobic interactions with the following amino acids: Trp340 (W6.48) and Phe343 (F6.51). The binding mode for ligands **2** and **12** corresponds to the results reported previously [15,17,20,26].

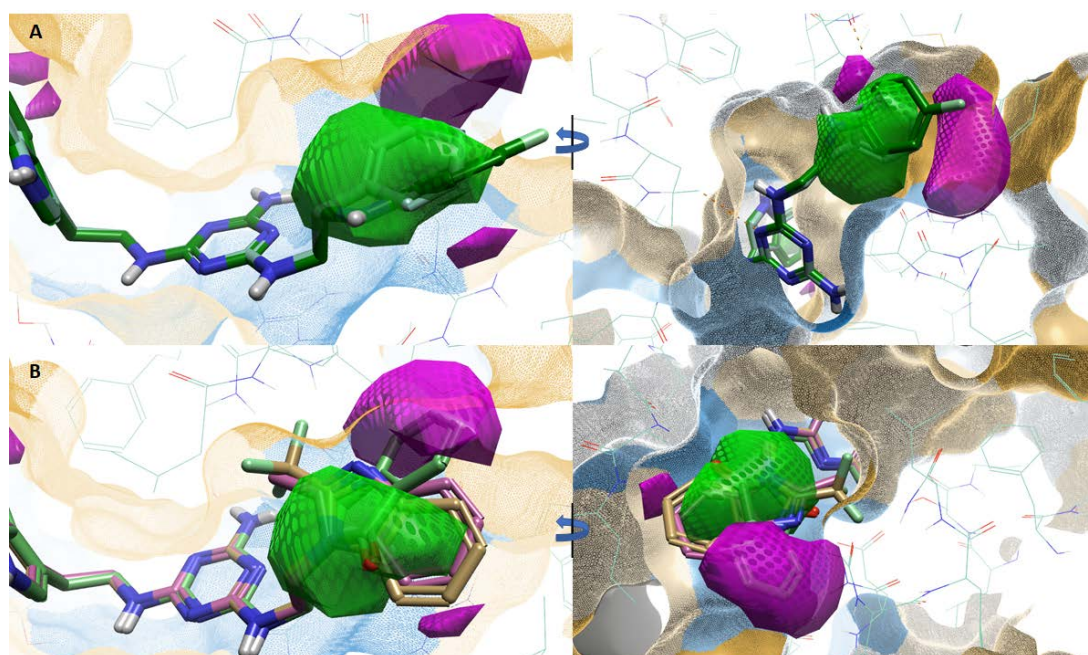


Figure 4. (A)—favorable (checked green)/unfavorable (checked magenta) hydrophobics for active ligands: 2 (teal) and 12 (green). (B)—favorable (checked green)/unfavorable (checked magenta) hydrophobics for representative, inactive ligands: 16 (light brown), 18 (pink), and 19 (light green). The orange area represents the hydrophobic surface of the receptor binding site, and the blue area represents the hydrophilic surface of the receptor binding site.

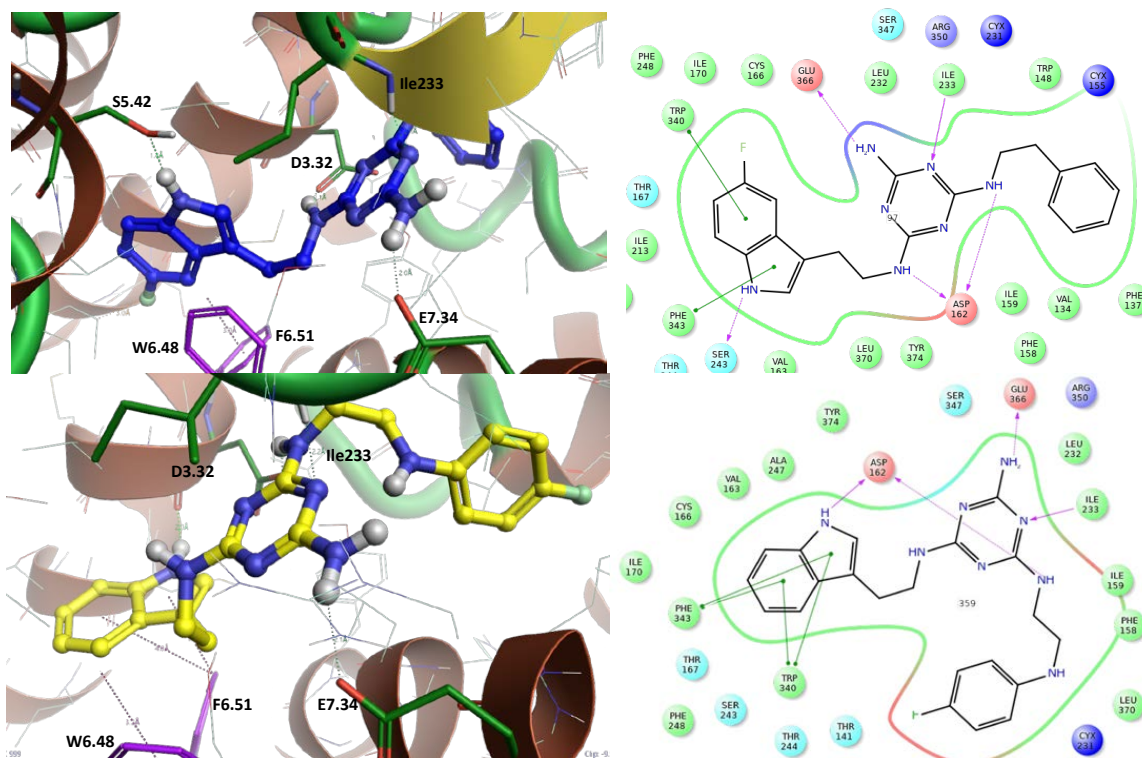


Figure 5. The left side represents the binding mode of ligand 2 (blue) and ligand 12 (yellow) in a homologous model of the 5-HT₇ receptor. Blue amino acids form hydrogen bonds, and purple amino acids represent π - π stacking hydrophobic interactions. The right side represents ligand–protein interactions.

2.5. Metabolic Stability

Highly active compounds **2** and **12** were submitted for metabolic stability evaluation tests using mouse liver microsomes (MLMs). UHPLC-MS analysis of the samples after compounds **2** and **12** were incubated for 2 h in the presence of MLMs showed that 20% and 29% of the original compound remained, respectively. Table 2 shows potential metabolic pathways for the tested compounds as well as Figure 6 shows possible main metabolites predicted by Metasite 6.0.1. It was found, based on the results, that the presence of fluorine at indole position C-5 (ligand **2**) did not have a significant effect on increased metabolic stability compared to the unsubstituted compound [20]. It seems, however, that substituents at the B ring of the ligands have a more important role. Compound **12**, containing a fluorine atom, was found to be more stable than compound **2** and the reference verapamil. The data correspond to our previous results [15], in which substituents at the B ring increased metabolic stability. Potential sites in the molecules sensitive to enzyme activity and leading to degradation were proposed using an in silico approach, also with MetaSite 6.0.1 (Figure 7).

Table 2. Metabolic stability summary: the molecular masses and metabolic pathways of compounds **2**, **12**, and verapamil (reference unstable drug) after incubation with mouse liver microsomes (MLMs). Main metabolic pathways are marked in red.

Substrate	Molecular Mass (m/z)	% Remaining	Molecular Mass of the Metabolite (m/z)	Metabolic Pathway
2	392.33	19.79	408.28 (M1)	hydroxylation
			406.28 (M2)	ketone formation
			424.29 (M3)	double hydroxylation
			390.27(M4)	dehydrogenation
			390.27 (M5)	dehydrogenation
			424.29 (M6)	double hydroxylation
			408.34 (M7)	hydroxylation
			422.30 (M8)	ketone formation and
			424.29 (M9)	hydroxylation
12	407.35	29.12	312.25 (M1)	decomposition
			423.30 (M2)	hydroxylation
			405.29 (M3)	dehydrogenation
			405.29 (M4)	dehydrogenation
			439.31 (M5)	double hydroxylation
			423.30 (M6)	hydroxylation
			405.02 (M7)	dehydrogenation
Verapamil *	455.54	23.93	441.42 (M1)	demethylation
			441.42 (M2)	demethylation
			291.35 (M3)	defragmentation
			293.34 (M4)	defragmentation/hydroxylation
			277.33 (M5)	defragmentation

[*] previously published [27].

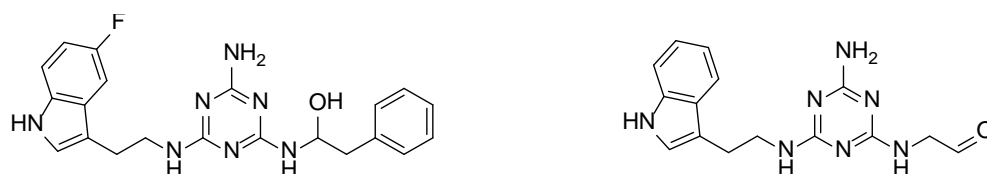


Figure 6. The proposed by MetaSite structure of hydroxylated main metabolite M1 of compound **2** (left) and decomposed main metabolite M1 of compound **12** (right).



Figure 7. The MetaSite 6.0.1. software prediction of the most probable sites of tested compounds metabolism-2 (**left**), **12** (**right**). The darker red color—the higher probability of being involved in the metabolism pathway. The blue circle marked the site of compound with the highest probability of metabolic bioconversion.

2.6. CYP3A4 Interaction

Potential drug–drug interactions (DDIs) are an important aspect that should be considered when designing new compounds. Isoenzyme CYP3A4 is one of the varieties of enzymes responsible for xenobiotic metabolism [28]. We evaluated active compounds **2** and **12** in terms of affinity toward this isoenzyme (Figure 8). Both compounds at concentrations identical to that of ketoconazole, the reference compound (1 μM) or lower were shown to have no or slight inhibition activity toward CYP3A4. Compound **2** at 10 μM showed moderate (%CYP3A4 activity = 50) and compound **12** showed high (%CYP3A4 activity = 20) inhibition effect, respectively. A very high inhibition effect was observed for both compounds at 25 μM (%CYP3A4 activity < 15).

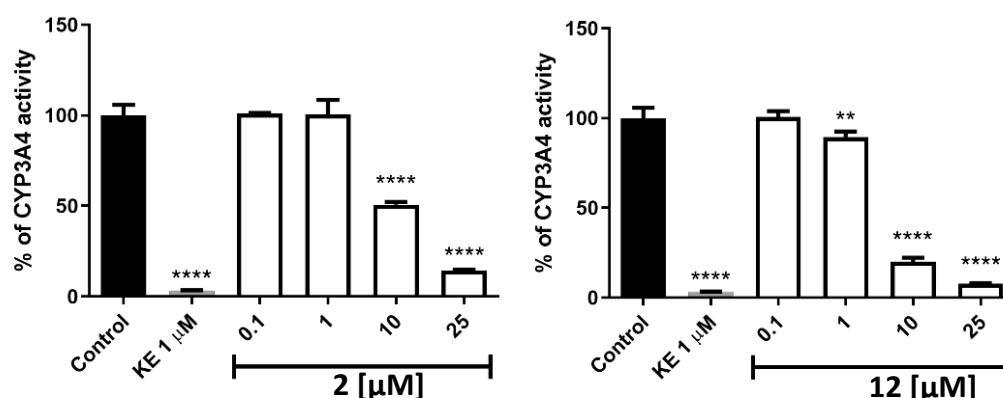


Figure 8. The influence of **2** (left), **12** (right), and ketoconazole (KE) on CYP3A4 activity. Statistical significance (** $p < 0.01$, **** $p < 0.0001$) was analyzed by Graph Pad Prism 8.0.1 software using One-way ANOVA and Bonferroni's Multiple Comparison Post Test in comparison with the negative control (100% of CYP3A4 activity). The compounds were examined in triplicate.

2.7. Hepatotoxicity

The tested compounds **2** and **12** were evaluated in terms of cytotoxicity against the HepG2 cell line to assess their hepatotoxic potential (Figure 9). It was an interesting finding that both compounds had proliferative activity in lower concentrations (<10 μM). A cytotoxic effect appeared only at 50 μM (**2**, % cell viability = 35; **12**, % cell viability = 20); at 100 μM , the cells were practically no viable.

2.8. In Vivo Cardiotoxicity

The compounds were evaluated for their ecotoxicity on the Danio rerio experimental model. OECD 236 test [29] with modifications was applied. Both compounds were found cardiotoxic within the non-toxic range, based on the heart rate measurement. For the compound **2**, 5 $\mu\text{g}/\text{mL}$ was found cardiotoxic (Figure 10) and for **12**, 7.5 $\mu\text{g}/\text{mL}$ (Figure 11). The results were confirmed by malformations observation. Pericardial edema (PE) was

observed at 5 $\mu\text{g}/\text{mL}$ for **2** (Figure 12) and at 7.5 $\mu\text{g}/\text{mL}$ for **12** (Figure 13). Moreover, scoliosis (S) and tail autophagy (TA) were also noted.

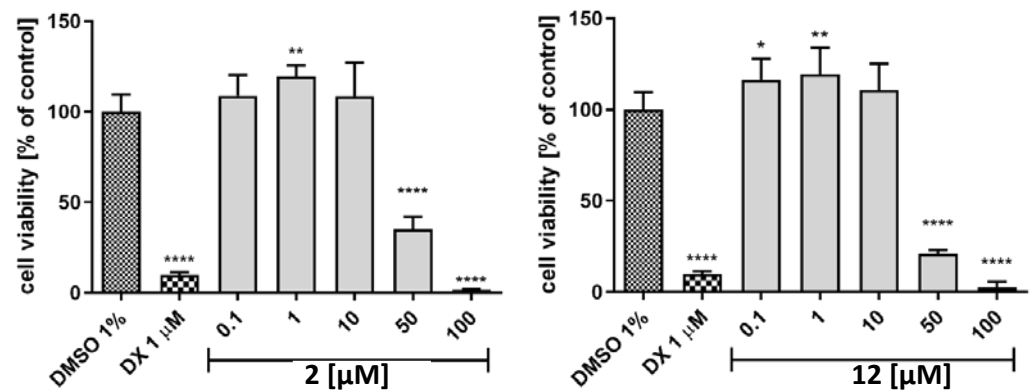


Figure 9. The effect of cytostatic drug doxorubicin and **2** (left), **12** (right) on hepatoma HepG2 cell line viability after 72 h of incubation at 37°, 5% CO₂. The statistical significance (GraphPad Prism 8.0.1) was evaluated by a one-way ANOVA, followed by Bonferroni's Comparison Test (* $p < 0.05$, ** $p < 0.01$, and **** $p < 0.0001$ compared with negative control DMSO 1% in growth media).

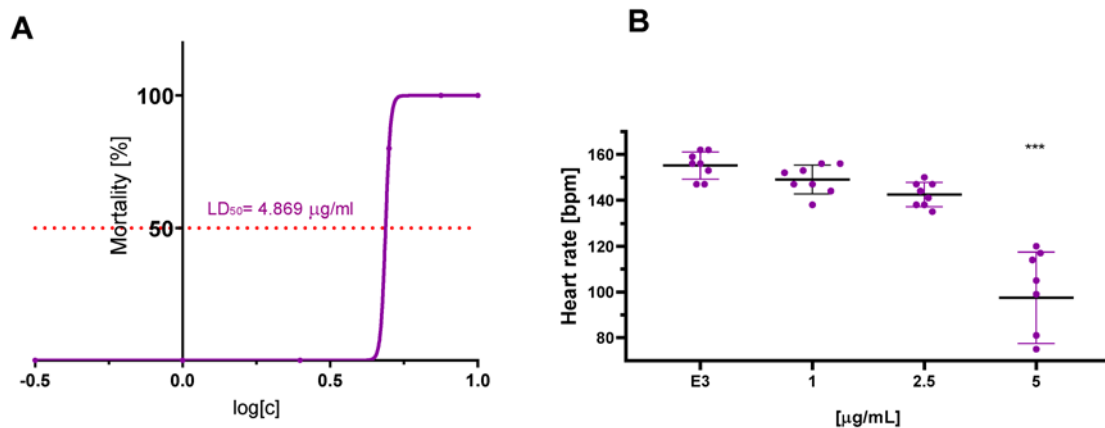


Figure 10. The effect of compound **2** on *Danio rerio*—(A). mortality and (B). cardiotoxicity after 96 h of incubation at 28 °C. The statistical significance (GraphPad Prism 8.0.1) was evaluated by a one-way ANOVA, followed by Tukey post hoc (***) $p < 0.001$ compared with negative control DMSO 1% in growth medium (E3).

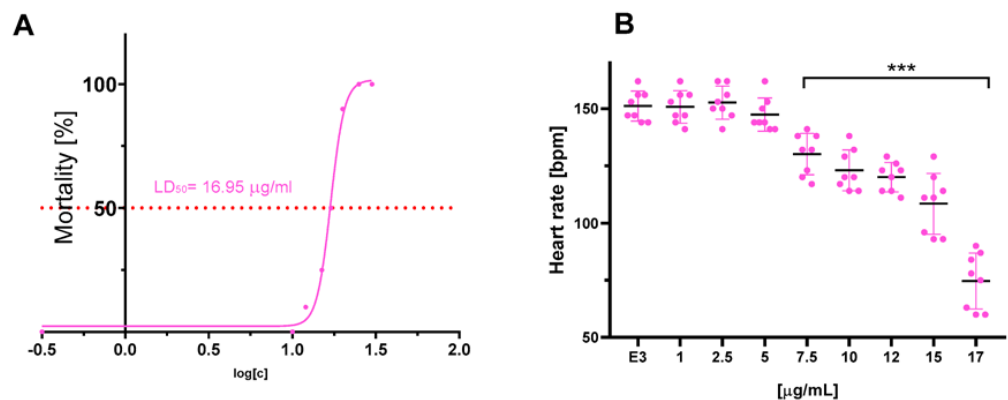


Figure 11. The effect of compound **12** on *Danio rerio*—(A). mortality and (B). cardiotoxicity after 96 h of incubation at 28 °C. The statistical significance (GraphPad Prism 8.0.1) was evaluated by a one-way ANOVA, followed by Tukey post hoc (***) $p < 0.001$ compared with negative control DMSO 1% in growth medium (E3).

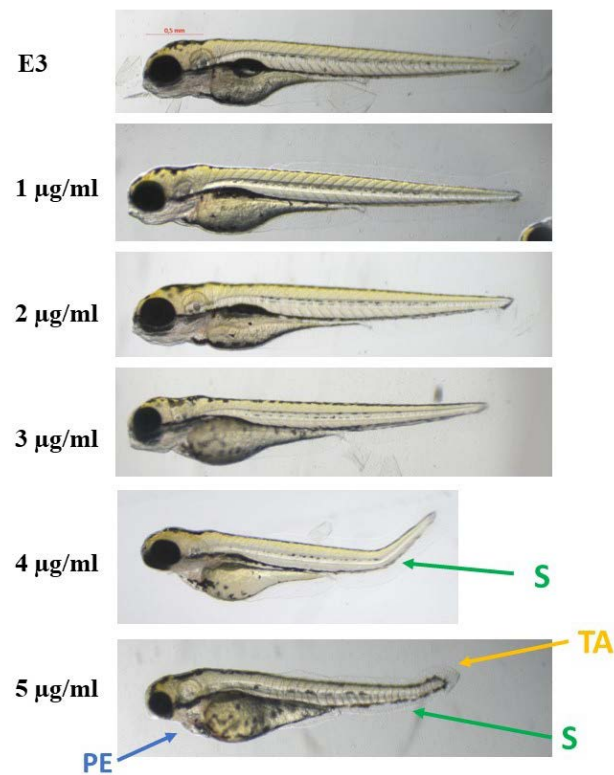


Figure 12. The effect of compound 2 on *Danio rerio* development after 96 h of incubation at 28 °C. PE—pericardial edema; S—scoliosis; TA—tail autophagy; E3—growth medium.

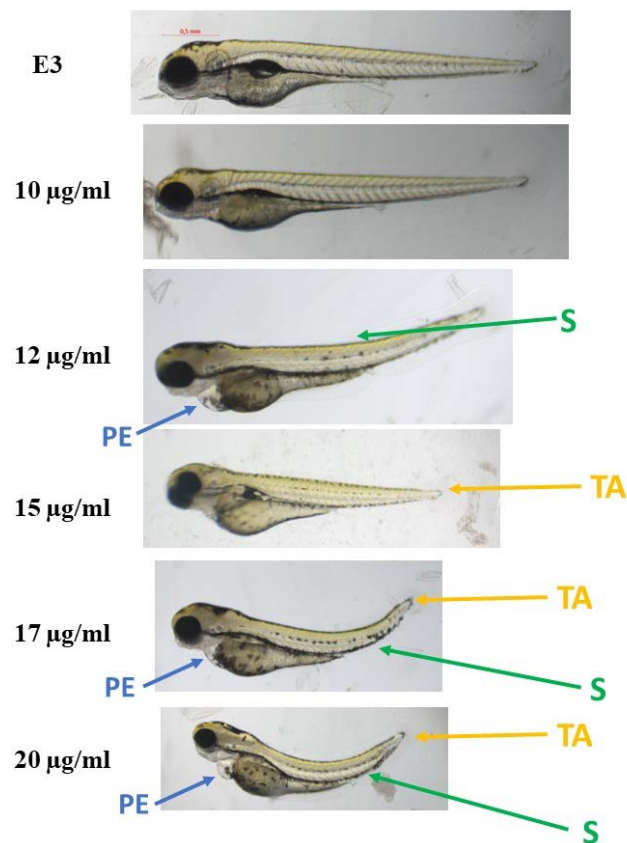


Figure 13. The effect of compound 12 on *Danio rerio* development after 96 h of incubation at 28 °C. PE—pericardial edema; S—scoliosis; TA—tail autophagy; E3—growth medium.

3. Discussion and Conclusions

In spite of the significant functions of the 5-HT₇ receptor [30] both in and outside the central nervous system and the recent progress in medicinal chemistry and pharmacology, a drug having selectivity toward 5-HT₇R is yet to be fully developed [30]. Taking this into consideration, the objective of this paper was to design ligands showing high activity and selectivity toward the 5-HT₇ receptor without incorporating the arylpiperazine pharmacophore, which may increase affinity to other aminergic GPCRs.

All finally synthesized compounds were obtained by a condensation reaction supported by microwave irradiation for 2.5 min with a yield of more than 50%. An interesting fact turned out to be the synthesis of ligands **8**, **12**, and **15**. So far, working on 1,3,5-triazines with indole motif [15,20], we have successfully used a mild alkaline agent, which was potassium carbonate, obtaining final products with medium or high yield. In the case of the mentioned ligands, the reactions did not proceed as it was expected, leading to the elimination of the ethyl bridge. The usage of a slightly weaker base, which was sodium carbonate, resulted in obtaining the desired products with good yield. It was found when studying type 1 compounds that incorporation of EWG or EDG substituents in most cases did not improve affinity toward the 5-HT₇ receptor in the majority of synthesized compounds. Compounds **1** and **3–6** had lower activity than the unsubstituted compound (Figure 1A). Ligand **2**, whose activity did not change compared to the unsubstituted compound, was an exception (Figure 1A). The fact may be accounted for by the effect of bioisosterism of the fluorine atom (hydrogen bioisostere). When exploring the aromatic region of the B ring, ligands with chlorine, fluorine, and methoxy substituents in the *ortho* position showed the lowest activity; higher activity was shown for the substituents in the *meta* position and the highest for substituents in the *para* position (ligand **12**, $K_i = 18$ nM). It is noted that ligands with small substituents (Cl, F) were more active than those with slightly larger substituents (OMe). The incorporation of much larger heterocyclic compounds (type 3) resulted in the loss of activity on the 5-HT₇ receptor. Type 4 compounds showed once more that the distance between the triazine core and the aromatic system, which should be two or three atoms, was crucial [15,20]. The SARs for the resulting compounds were supported using 3D-QSAR computed methods. The bioconformation and the binding mode for the two best compounds (**2** and **12**) were determined using molecular modeling (docking), and the results were consistent with our previous reports [15,20]. The tested ligands (**2** and **12**) are 5-HT₇ receptor antagonists, have moderate metabolic activity (higher or similar to verapamil and still higher than unsubstituted ligands which were described in our publication [20]), and moderate or weak potential drug-drug interactions with respect to ketoconazole. As for hepatotoxicity, both compounds at more than 50 μ M showed cytotoxicity against the HepG2 cell line. The ecotoxicity tests with the use of *Daio rerio* as a model organism turned out **2** to be more toxic than **12**. Moreover, cardiotoxicity expressed as heart rate abnormalities was observed at higher doses for **2** than **12**, and it suggests that cardiotoxic potential needs to be reduced in the future.

4. Materials and Methods

4.1. Chemistry

4.1.1. General

All primary substrates were purchased commercially from Sigma-Aldrich (St. Louis, MO, USA). The solvents used for column chromatography (purchased from Merck, Kenilworth, NJ, USA), thin layer chromatography (TLC), and preparative thin layer chromatography (pTLC) had purity above 99.5%. ¹H and ¹³C NMR spectra were recorded using Bruker 400 MHz systems with TMS as an internal standard. Melting points were determined with the Bötetius apparatus. HPLC–MS analyses were performed on the Shimadzu Nexera XR system equipped with PDA (SPD-M40) and LCMS-2020 detectors. Analyses were performed on Phenomenex XB-C18 1.7 μ m (50 \times 2.1 mm) (method A) column with gradient of solvents as a mobile phase: Solvent A (0.01% HCOOH in water) and B (0.01% HCOOH in methanol); t = 0 min, 10% of B, t = 4 min, 90% of B, t = 6 min, 90% of B,

$t = 6.1$ min 10% of B, stop time 11 min or Phenomenex C18 $1.7 \mu\text{m}$ (50×2.1 mm) (method B) column with gradient of solvents as a mobile phase: solvent A (0.01% HCOOH in water) and solvent B (0.01% HCOOH in MeOH): $t = 0$ min 5% of B, $t = 3$ min 90% of B, $t = 4$ min 90% of B, $t = 4.5$ min 5% of B stop time 7 min; flow rate 0.4 mL min^{-1} ; the UV-VIS detection was performed in a range of 240–700 nm, the MS data were collected in ESI + mode in a range of m/z 100–800 with scan speed $15,000 \text{ u/s}$ and event time 0.1 s. Analytical thin-layer chromatography (TLC) was performed using 0.2 mm silica gel precoated aluminum sheets (60 F254, Merck), and UV light at 254 nm was used for visualization. Preparative thin-layer chromatography (pTLC) was performed using 2000 μm silica gel precoated glass backed (F254, Silicycle). A CEM Discover™ Focused Microwave System at 50 W power was used for all microwave-assisted reactions in order to obtain final compounds. Within 2.5 min of reaction with a power of 50 W, the temperature increased up to $120 \text{ }^\circ\text{C}$, while the pressure increased up to 9 bar. Characterization of the intermediates and spectra for the final compounds can be found in Supporting Information.

4.1.2. General Procedure for the Synthesis of Compounds 29–34

12 mL of DMF was cooled to $0 \text{ }^\circ\text{C}$, and phosphoryl chloride (38.5 mmol) was added dropwise. In this temperature solution of commercially available indoles 23–28 (35.5 mmol) in 3 mL of DMF was added dropwise, and the resulting mixture was stirred at room temperature for one hour. The reaction became a thick, pale suspension. Sodium hydroxide solution (10%, 40 mL) was added slowly to the reaction mixture ($\text{pH} = 13\text{--}14$), followed by precipitation of pale solid 29–34. The solid was filtered, rinsed with distilled water, and dried.

4.1.3. General Procedure for the Synthesis of Compounds 35–40

Intermediate 29–34 (23.5 mmol) was placed in a one-necked round bottom flask and dissolved in 60 mL nitromethane, and then, ammonia acetate (44.2 mmol) was added. The mixture was reacted in a microwave reactor at 80 W ($100 \text{ }^\circ\text{C}$) for 20 min. Reaction progress was monitored via TLC (hexane:EtOAc 1:1 v/v). After this time, TLC indicated full conversion of starting material, and the mixture was cooled to room temperature with precipitation of yellow solid 35–40. The solid was filtered, rinsed with distilled water, and dried.

4.1.4. Synthesis of 3-(2-Nitroethyl)-1H-Indole-5-Carbonitrile (41)

Intermediate 35 (4.1 g, 19.2 mmol) was dissolved in the 330 mL mixture of DMF:MeOH (1:1, v/v), followed by the addition of sodium borohydride (8 g, 21.1 mmol). The mixture was stirred at room temperature for 5 h. Reaction progress was monitored via TLC (hexane:EtOAc 1:1 v/v). After reaction completion reaction was diluted with 2M HCl to reach $\text{pH} = 7$. The solvent was reduced and extracted with EtOAc (3×150 mL). The crude product was triturated with a mixture of MeOH:chloroform to yield 2.17 g of the titled compound. The mother liquor was concentrated to dryness and purified at column chromatography eluted with hexane:EtOAc (v/v) 8:2 \rightarrow 6:4 to yield 0.8 g of the titled compound. Creamy solid (71% yield); mp.: $131\text{--}133 \text{ }^\circ\text{C}$ (ref. $134\text{--}136 \text{ }^\circ\text{C}$ [31]); method B: ESI+MS calc. for $\text{C}_{11}\text{H}_9\text{N}_3\text{O}_2$ $m/z = 215$; found $m/z = 214$ $[\text{M-H}]^-$.

4.1.5. General Procedure for the Synthesis of Compounds 42–46

Lithium aluminum hydride (25.9 mmol) was placed in a three-necked round bottom flask, followed by the addition of 20 mL dry THF. The resulting suspension was cooled to $0 \text{ }^\circ\text{C}$, and mixture of intermediates 36–40 (4.7 mmol) in 20 mL THF was added dropwise. The mixture was stirred at room temperature for 72 h and then quenched with slow addition of mixture $\text{H}_2\text{O}:\text{MeOH}$ (9:1, v/v). The suspension was filtered by a Celite bed, and pH-dependent extraction was performed: filtrate was acidified to reach $\text{pH} 2\text{--}3$ with 1 M HCl, followed by extraction with EtOAc (3×100 mL). The water layer was alkalized to reach

pH 10 with 1 M NaOH and then extracted with EtOAc (3 × 100 mL). Organic layers were combined, dried over MgSO₄, and concentrated to yield brown, sticky oil **42–46**.

4.1.6. Synthesis of 3-(2-Aminoethyl)-1H-Indole-5-Carbonitrile (**47**)

A solution of **41** (1.5 g, 6.9 mmol) in 205 mL MeOH was added to the solution of zinc (10.4 g, 0.16 mol) in 205 mL 2M HCl and refluxed for 1.5 h. After this time mixture was cooled to room temperature and filtered. The filtrate was alkalized to pH 12, and MeOH was removed under reduced pressure. The resulting mixture was extracted with EtOAc (3 × 200 mL), and organic layers were combined, dried over MgSO₄ then evaporated to dryness. It obtained 0.87 g (67% yield) of titled compound **47**, which was used in the next step without any further purification.

4.1.7. Synthesis of 4,6-Dichloro-N-Phenethyl-1,3,5-Triazin-2-Amine (**50**)

To a solution of cynuric chloride **48** (8.35 g, 45.2 mmol) in 100 mL THF cooled to 0 °C, a solution of phenylethylamine **49** (5 g, 41.2 mmol) in 5 mL THF was added dropwise. The reaction was carried out at 0–3 °C for 2 h. The resulting precipitate was filtered, and the filtrate was diluted with 0.1 M HCl and extracted with chloroform (3 × 100 mL). Organic layers were combined, dried over MgSO₄, and concentrated to yield a brown solid. The solid was triturated with acetone and then filtered. The black filtrate was purified using column chromatography eluted with hexane:EtOAc (*v/v*) 9:1-> 6:4 to yield 3.74 g of the titled compound. Creamy solid (34% yield); method B: ESI-MS calc. for C₁₁H₁₀Cl₂N₄ *m/z* = 268.0; found *m/z* = 269.1 [M+H]⁺.

4.1.8. Synthesis of 6-Chloro-N²-Phenethyl-1,3,5-Triazine-2,4-Diamine (**51**)

Briefly, **50** (3.5 g, 13.0 mmol) was dissolved in 50 mL acetone, followed by the addition of 5.7 mL 25% ammonia solution. The reaction was carried out at room temperature for 5 h. The resulting precipitate was filtered, and the filtrate evaporated to dryness, yielding 2.8 g of titled compound **51**. Creamy solid (86% yield); ESI-MS calc. for C₁₁H₁₂ClN₅ *m/z* = 249; method B: found *m/z* = 250 [M+H]⁺.

4.1.9. General Procedure for the Synthesis of Final Compounds **1–6** (Microwave-Assisted)

Briefly, **51** (0.25 g, 1.0 mmol), potassium carbonate (0.41 g, 3.0 mmol), and TBAB (0.032 g, 0.1 mmol) were ground in a mortar and transferred to a sealed tube which was previously charged with appropriate amine **42–47** (2.5 mmol). Subsequently, 5 wt % DMF was added. The mixture was reacted in a microwave reactor at 50 W for 2.5 min. Reaction progress was monitored via TLC (chloroform: MeOH 9:1 *v/v*). The mixture was cooled down and extracted with chloroform (3 × 20 mL). Organic layers were combined, dried over MgSO₄, and concentrated. The crude product was purified via column chromatography with elution using chloroform then chloroform:MeOH (*v/v*) 99:1-> 97:3. The white or beige sticky oil was then dissolved in acetone and pH was adjusted to 2–3 with 4 M HCl in 1,4-dioxane. The resulting mixture was crushed by the addition of cold diethyl ether, then the white or beige powder was filtered and rinsed with cold diethyl ether and then dried to yield final product **1–6**.

4.1.10. 3-(2-((4-Amino-6-(Phenethylamino)-1,3,5-Triazin-2-yl)Amino)Ethyl)-1H-Indole-5-Carbonitrile Hydrochloride (**1**)

Beige solid (54% yield), mp: 95–98 °C; ¹H NMR (600 MHz, MeOD) δ 8.02 (s, 1H), 7.51 (d, J = 8.4 Hz, 1H), 7.40 (t, J = 9.9 Hz, 1H), 7.34–7.15 (m, 6H), 3.76–3.70 (m, 2H), 3.64 (t, J = 7.0 Hz, 1H), 3.59 (t, J = 7.1 Hz, 1H), 3.09 (t, J = 7.0 Hz, 2H), 2.91 (d, J = 7.3 Hz, 1H), 2.86 (t, J = 7.1 Hz, 1H); ¹³C NMR (151 MHz, MeOD) δ 156.0, 138.6, 138.5, 128.4, 128.1, 128.1, 127.3, 126.0, 125.1, 125.1, 123.8, 123.7, 120.5, 112.9, 112.1, 100.9, 42.0, 41.3, 35.0, 24.5; HPLC-MS analysis t_r = 5.84 min (94% purity, method A), calc. for C₂₂H₂₂N₈ *m/z* = 398.2, found *m/z* = 399.2 [M+H]⁺.

4.1.11. N²-(2-(5-Fluoro-1H-Indol-3-yl)ethyl)-N⁴-Phenethyl-1,3,5-Triazine-2,4,6-Triamine Hydrochloride (2)

Beige solid (67% yield), mp: 110–114 °C; ¹H NMR (600 MHz, MeOD) δ 7.33–7.29 (m, 2H), 7.27–7.14 (m, 6H), 6.87 (t, J = 7.9 Hz, 1H), 3.76–3.67 (m, 2H), 3.63 (t, J = 6.2 Hz, 1H), 3.60 (t, J = 7.2 Hz, 1H), 3.03 (t, J = 6.5 Hz, 2H), 2.90 (t, J = 6.8 Hz, 1H), 2.86 (t, J = 7.1 Hz, 1H); ¹³C NMR (151 MHz, MeOD) δ 158.2, 156.7, 156.1, 133.3, 132.2, 131.0, 128.5, 128.1, 126.0, 124.3, 111.7, 109.1, 108.9, 102.5, 102.3, 42.0, 41.3, 35.0, 24.8; HPLC-MS analysis t–6.13 min (99% purity, method A), calc. for C₂₁H₂₂FN₇ m/z = 391.2, found m/z = 392.2 [M+H]⁺.

4.1.12. N²-(2-(5-Bromo-1H-Indol-3-yl)ethyl)-N⁴-Phenethyl-1,3,5-Triazine-2,4,6-Triamine Hydrochloride (3)

Beige solid (63% yield), mp: 82–85 °C; ¹H NMR (600 MHz, MeOD) δ 7.70 (d, J = 13.1 Hz, 1H), 7.33–7.17 (m, 8H), 3.71 (t, J = 7.2 Hz, 2H), 3.64 (t, J = 7.2 Hz, 1H), 3.60 (t, J = 7.1 Hz, 1H), 3.02 (dd, J = 12.8, 5.8 Hz, 2H), 2.91 (t, J = 7.2 Hz, 1H), 2.87 (t, J = 7.0 Hz, 1H); ¹³C NMR (151 MHz, MeOD) δ 156.1, 138.7, 135.4, 129.2, 128.4, 128.1, 128.1, 126.1, 126.0, 123.9, 123.6, 120.4, 112.6, 111.5, 111.4, 66.98, 47.2, 42.0, 41.4, 35.0, 24.7; HPLC-MS analysis t–6.41 min (98% purity, method A), calc. for C₂₁H₂₂⁷⁹BrN₇ m/z = 451.1, found m/z = 452.2 [M+H]⁺, calc. for C₂₁H₂₂⁸¹BrN₇ m/z = 453.1, found m/z = 454.2 [M+H]⁺.

4.1.13. N²-(2-(5-Chloro-1H-Indol-3-yl)ethyl)-N⁴-Phenethyl-1,3,5-Triazine-2,4,6-Triamine Hydrochloride (4)

White solid (58% yield), mp: 106–108 °C; ¹H NMR (600 MHz, MeOD) δ 7.55 (d, J = 12.2 Hz, 1H), 7.32 (dd, J = 17.0, 8.0 Hz, 2H), 7.28–7.15 (m, 5H), 7.07 (dd, J = 8.5, 1.7 Hz, 1H), 3.74–3.67 (m, 2H), 3.64 (t, J = 7.2 Hz, 1H), 3.60 (t, J = 7.1 Hz, 1H), 3.04 (t, J = 7.0 Hz, 2H), 2.91 (t, J = 7.3 Hz, 1H), 2.87 (t, J = 7.1 Hz, 1H); ¹³C NMR (151 MHz, MeOD) δ 156.0, 138.6, 135.1, 128.5, 128.5, 128.4, 128.1, 128.1, 126.0, 124.0, 121.1, 117.3, 117.2, 112.1, 111.4, 42.0, 41.4, 35.0, 24.7; HPLC-MS analysis t–6.11 min (94% purity, method A), calc. for C₂₁H₂₂³⁵ClN₇ m/z = 407.2, found m/z = 408.4 [M+H]⁺, calc. for C₂₁H₂₂³⁷ClN₇ m/z = 409.2, found m/z = 410.4 [M+H]⁺.

4.1.14. N²-(2-(5-Methoxy-1H-Indol-3-yl)ethyl)-N⁴-Phenethyl-1,3,5-Triazine-2,4,6-Triamine Hydrochloride (5)

White solid (52% yield), mp: 111–115 °C; ¹H NMR (600 MHz, MeOD) δ 7.31 (t, J = 7.4 Hz, 2H), 7.27–7.21 (m, 4H), 7.18 (d, J = 7.5 Hz, 1H), 7.07 (t, J = 20.0 Hz, 1H), 6.78 (t, J = 8.3 Hz, 1H), 3.83 (d, J = 4.2 Hz, 1H), 3.76 (s, 3H), 3.70 (t, J = 6.7 Hz, 1H), 3.66–3.61 (m, 1H), 3.57 (t, J = 7.3 Hz, 1H), 3.05 (dd, J = 14.5, 7.3 Hz, 2H), 2.90 (t, J = 7.2 Hz, 1H), 2.85 (t, J = 7.3 Hz, 1H); ¹³C NMR (151 MHz, MeOD) δ 156.0, 153.5, 138.6, 132.0, 128.4, 128.1, 128.1, 127.6, 126.1, 126.0, 123.0, 111.5, 111.3, 111.2, 111.1, 54.9, 42.0, 41.5, 35.0, 24.8; HPLC-MS analysis t–5.91 min (98% purity, method A), calc. for C₂₂H₂₅N₇O m/z = 403.2, found m/z = 404.2 [M+H]⁺.

4.1.15. N²-(2-(5-Methyl-1H-Indol-3-yl)ethyl)-N⁴-Phenethyl-1,3,5-Triazine-2,4,6-Triamine Hydrochloride (6)

White solid (57% yield), mp: 118–121 °C; ¹H NMR (600 MHz, MeOD) δ 7.31 (dd, J = 15.8, 8.7 Hz, 2H), 7.28–7.21 (m, 4H), 7.18 (t, J = 6.2 Hz, 1H), 7.06 (d, J = 21.7 Hz, 1H), 6.94 (dd, J = 12.1, 8.5 Hz, 1H), 3.75 (t, J = 7.1 Hz, 1H), 3.70 (bs, 1H), 3.63 (bs, 1H), 3.56 (t, J = 7.3 Hz, 1H), 3.05 (t, J = 6.7 Hz, 2H), 2.90 (t, J = 7.2 Hz, 1H), 2.85 (t, J = 7.3 Hz, 1H), 2.38 (s, 3H)–hydrogen bonded rotamer H₃C-C_{Ar}; ¹³C NMR (151 MHz, MeOD) δ 156.0, 138.6, 135.1, 128.5, 128.4, 128.1, 128.1, 127.6, 127.3, 126.1, 126.0, 122.6, 122.3, 117.4, 110.6, 42.0, 41.5, 35.1, 24.9, 20.3 (H₃C-C_{Ar}). HPLC-MS analysis t–6.00 min (98% purity, method A), calc. for C₂₂H₂₅N₇ m/z = 387.2, found m/z = 388.4 [M+H]⁺.

4.1.16. General Procedure for the Synthesis of Compounds 61–68

In a round bottom flask, 2-chloroethanamine hydrochloride **52** (1.0 g, 8.6 mmol) was suspended in 8 mL of toluene. To the resulting mixture, appropriate aniline **53–60** (51.7 mmol) was added, and the mixture was refluxed for 20 h. After this period, toluene was evaporated, and residues were triturated with dichloromethane to yield solid as titled compounds **61–68** (optionally solid may be washed with diethyl ether).

4.1.17. General Procedure for the Synthesis of Final Compounds 7, 9–11, and 14 (microwave-assisted)

Briefly, **69** [20] (0.25 g, 0.8 mmol), amines **61, 63–65, 67** (2.0 mmol) potassium carbonate (0.36 g, 2.5 mmol) and TBAB (0.032 g, 0.1 mmol) were ground in a mortar and transferred to a sealed tube. Subsequently, 5 wt % DMF was added. The mixture was reacted in a microwave reactor at 50 W for 2.5 min. Reaction progress was monitored via TLC (chloroform: MeOH 9:1 *v/v*). The mixture was cooled down and extracted with chloroform (3 × 20 mL). Organic layers were combined, dried over MgSO₄, and concentrated. The crude product was purified via column chromatography with elution using chloroform then chloroform:MeOH (*v/v*) 99:1 → 97:3. Colorless sticky oil was then dissolved in acetone, and pH was adjusted to 2–3 with 4 M HCl in 1,4-dioxane. The resulting mixture was crushed by the addition of cold diethyl ether, and then the white or beige powder was filtered and rinsed with cold diethyl ether and then dried to yield final products **7, 9–11, and 14**.

4.1.18. N²-(2-(1H-Indol-3-yl)ethyl)-N⁴-(2-((2-Chlorophenyl)amino)ethyl)-1,3,5-Triazine-2,4,6-Triamine Hydrochloride (7)

White solid (72% yield), mp: 105–108 °C; ¹H NMR (600 MHz, MeOD) δ 7.56 (dd, J = 19.1, 7.7 Hz, 1H), 7.35 (d, J = 8.1 Hz, 1H), 7.33–6.99 (m, 5H), 6.99–6.87 (m, 1H), 6.82–6.66 (m, 1H), 3.72 (dd, J = 15.3, 7.2 Hz, 2H), 3.66 (dd, J = 13.3, 6.3 Hz, 1H), 3.54 (t, J = 6.0 Hz, 1H), 3.49 (t, J = 5.9 Hz, 1H), 3.41 (t, J = 6.1 Hz, 1H), 3.07 (t, J = 6.4 Hz, 1H), 3.03 (t, J = 7.0 Hz, 1H); ¹³C NMR (151 MHz, MeOD) δ 156.0, 142.0, 136.8, 129.1, 127.7, 127.3, 122.3, 121.0, 119.8, 118.9, 118.3, 118.2, 117.7, 112.8, 111.3, 110.9, 43.3, 41.4, 38.8, 24.8; HPLC-MS analysis t–5.92 min (98% purity, method A), calc. for C₂₁H₂₃³⁵ClN₈ *m/z* = 422.2, found *m/z* = 423.2 [M+H]⁺, calc. for C₂₁H₂₃³⁷ClN₈ *m/z* = 424.2, found *m/z* = 425.2 [M+H]⁺.

4.1.19. N²-(2-(1H-Indol-3-yl)ethyl)-N⁴-(2-((4-Chlorophenyl)amino)ethyl)-1,3,5-Triazine-2,4,6-Triamine Hydrochloride (9)

White solid (70% yield), mp: 97–100 °C; ¹H NMR (600 MHz, MeOD) δ 7.58 (d, J = 7.8 Hz, 1H), 7.54–7.46 (m, 2H), 7.43 (d, J = 8.7 Hz, 1H), 7.36 (d, J = 8.0 Hz, 2H), 7.12 (dd, J = 18.5, 13.7 Hz, 2H), 7.03 (dt, J = 14.8, 7.5 Hz, 1H), 3.79–3.73 (m, 2H), 3.71 (t, J = 6.9 Hz, 1H), 3.58 (d, J = 5.2 Hz, 1H), 3.56 (d, J = 5.2 Hz, 1H), 3.16 (d, J = 18.8 Hz, 1H), 3.09 (t, J = 7.0 Hz, 1H), 3.04 (t, J = 6.9 Hz, 1H); ¹³C NMR (151 MHz, MeOD) δ 156.1, 136.8, 129.9, 127.3, 123.0, 122.8, 122.4, 122.3, 121.0, 118.3, 117.7, 117.7, 111.2, 111.0, 110.9, 41.3, 41.2, 36.8, 24.8; HPLC-MS analysis t–5.94 min (92% purity, method A), calc. for C₂₁H₂₃³⁵ClN₈ *m/z* = 422.2, found *m/z* = 423.4 [M+H]⁺, calc. for C₂₁H₂₃³⁷ClN₈ *m/z* = 424.2, found *m/z* = 425.4 [M+H]⁺.

4.1.20. N²-(2-(1H-Indol-3-yl)ethyl)-N⁴-(2-((2-Fluorophenyl)amino)ethyl)-1,3,5-Triazine-2,4,6-Triamine Hydrochloride (10)

White solid (70% yield), mp: 94–97 °C; ¹H NMR (600 MHz, MeOD) δ 7.60–7.52 (m, 1H), 7.36 (d, J = 8.1 Hz, 1H), 7.34–6.95 (m, 7H), 3.74 (t, J = 6.8 Hz, 3H), 3.61–3.54 (m, 2H), 3.48 (t, J = 6.1 Hz, 1H), 3.08 (t, J = 6.8 Hz, 1H), 3.04 (t, J = 7.0 Hz, 1H); ¹³C NMR (151 MHz, MeOD) δ 158.5, 156.1, 136.8, 127.3, 127.2, 125.0, 124.9, 122.4, 122.3, 121.0, 118.2, 117.7, 115.4, 115.3, 111.3, 110.9, 45.4, 41.3, 38.0, 24.8; HPLC-MS analysis t–5.79 min (99% purity, method A), calc. for C₂₁H₂₃FN₈ *m/z* = 406.2, found *m/z* = 407.4 [M+H]⁺.

4.1.21. N²-(2-(1H-Indol-3-yl)ethyl)-N⁴-(2-((3-Fluorophenyl)amino)ethyl)-1,3,5-Triazine-2,4,6-Triamine Hydrochloride (11)

White solid (52% yield), mp: 74–79 °C; ¹H NMR (600 MHz, MeOD) δ 7.58 (d, J = 7.8 Hz, 1H), 7.35 (d, J = 8.1 Hz, 1H), 7.10 (t, J = 7.5 Hz, 2H), 7.02 (bs, 2H), 6.46–6.23 (m, 3H), 3.67 (bs, 2H), 3.53 (bs, 2H), 3.28 (t, J = 6.3 Hz, 2H), 3.04 (t, J = 7.1 Hz, 2H); ¹³C NMR (151 MHz, MeOD) δ 165.0, 163.4, 136.8, 129.8, 127.3, 122.2, 120.9, 118.2, 117.9, 111.7, 110.8, 108.2, 102.3, 102.1, 98.5, 98.3, 42.8, 41.1, 39.4, 25.0; HPLC-MS analysis t–5.75 min (94% purity, method A), calc. for C₂₁H₂₃FN₈ m/z = 406.2, found m/z = 407.3 [M+H]⁺.

4.1.22. N²-(2-(1H-Indol-3-yl)ethyl)-N⁴-(2-((3-Methoxyphenyl)amino)ethyl)-1,3,5-Triazine-2,4,6-Triamine Hydrochloride (14)

White solid (77% yield), mp: 140–143 °C; ¹H NMR (600 MHz, MeOD) δ 7.58 (d, J = 7.8 Hz, 1H), 7.51 (d, J = 7.9 Hz, 1H), 7.44 (d, J = 17.4 Hz, 1H), 7.36 (d, J = 7.6 Hz, 2H), 7.17–7.07 (m, 3H), 7.06–6.98 (m, 1H), 3.85 (s, 3H), 3.80 (s, 3H), 3.59 (dd, J = 5.3, 4.0 Hz, 2H), 3.08 (t, J = 6.9 Hz, 2H), 3.03 (t, J = 6.9 Hz, 1H); ¹³C NMR (151 MHz, MeOD) δ 160.9, 156.1, 136.8, 130.7, 130.7, 127.3, 127.2, 122.5, 122.4, 121.0, 118.3, 117.8, 117.7, 111.2, 111.0, 110.9, 54.8, 41.3, 41.2, 36.6, 24.8; HPLC-MS analysis t–5.58 min (99% purity, method A), calc. for C₂₂H₂₆N₈O m/z = 418.2, found m/z = 419.4 [M+H]⁺.

4.1.23. General Procedure for the Synthesis of Final Compounds 8, 12, and 15 (Microwave-Assisted)

Briefly, **69** [20] (0.25 g, 0.8 mmol), amines **62**, **66**, and **68** (2.0 mmol), sodium carbonate (0.26 g, 2.5 mmol) and TBAB (0.032 g, 0.1 mmol) were ground in a mortar and transferred to a sealed tube. Subsequently, 5 wt % DMF was added. The mixture was reacted in a microwave reactor at 50 W for 2.5 min. Reaction progress was monitored via TLC (chloroform: MeOH 9:1 v/v). The mixture was cooled down and extracted with chloroform (3 × 20 mL). Organic layers were combined, dried over MgSO₄, and concentrated. The crude product was purified via column chromatography with elution using chloroform then chloroform:MeOH (v/v) 99:1→97:3. Colorless sticky oil was then dissolved in acetone, and pH was adjusted to 2–3 with 4 M HCl in 1,4-dioxane. The resulting mixture was crushed by the addition of cold diethyl ether; then, the white or beige powder was filtered and rinsed with cold diethyl ether then dried to yield final products **8**, **12**, and **15**.

4.1.24. N²-(2-(1H-Indol-3-yl)ethyl)-N⁴-(2-((3-Chlorophenyl)amino)ethyl)-1,3,5-Triazine-2,4,6-Triamine Hydrochloride (8)

White solid (70% yield), mp: 77–82 °C; ¹H NMR (600 MHz, MeOD) δ 7.58 (d, J = 7.8 Hz, 1H), 7.35 (d, J = 8.1 Hz, 1H), 7.10 (t, J = 7.8 Hz, 2H), 7.05–6.92 (m, 2H), 6.73–6.51 (m, 3H), 3.68 (s, 2H), 3.53 (s, 2H), 3.28 (t, J = 5.7 Hz, 2H), 3.04 (t, J = 7.1 Hz, 2H); ¹³C NMR (151 MHz, MeOD) δ 150.0, 136.8, 134.4, 129.8, 127.3, 122.2, 122.2, 121.0, 120.9, 118.2, 117.9, 115.8, 111.7, 111.5, 110.8, 110.6, 42.5, 41.1, 39.4, 25.0; HPLC-MS analysis t–5.60 min (100% purity, method A), calc. for C₂₁H₂₃³⁵ClN₈ m/z = 422.2, found m/z = 423.2 [M+H]⁺, calc. for C₂₁H₂₃³⁷ClN₈ m/z = 424.2, found m/z = 425.2 [M+H]⁺.

4.1.25. N²-(2-(1H-Indol-3-yl)ethyl)-N⁴-(2-((4-Fluorophenyl)amino)ethyl)-1,3,5-Triazine-2,4,6-Triamine Hydrochloride (12)

White solid (81% yield), mp: 140–143 °C; ¹H NMR (600 MHz, MeOD) δ 7.60 (dd, J = 17.7, 5.8 Hz, 2H), 7.52 (dd, J = 20.8, 8.3 Hz, 1H), 7.38–7.28 (m, 2H), 7.22 (t, J = 8.5 Hz, 1H), 7.12 (dd, J = 20.8, 13.1 Hz, 2H), 7.03 (dt, J = 15.0, 7.5 Hz, 1H), 3.79 (d, J = 5.3 Hz, 1H), 3.77–3.72 (m, 2H), 3.69 (d, J = 3.3 Hz, 1H), 3.59 (dd, J = 10.3, 4.5 Hz, 2H), 3.09 (t, J = 7.0 Hz, 1H), 3.05 (t, J = 6.9 Hz, 1H); ¹³C NMR (151 MHz, MeOD) δ 156.2, 136.8, 127.3, 124.3, 122.4, 122.3, 121.0, 118.3, 117.7, 117.7, 116.9, 116.8, 111.2, 111.0, 110.9, 41.3, 41.2, 36.5, 24.8; HPLC-MS analysis t–5.61 min (100% purity, method A), calc. for C₂₁H₂₃FN₈ m/z = 406.2, found m/z = 407.3 [M+H]⁺.

4.1.26. N²-(2-(1H-Indol-3-yl)ethyl)-N⁴-(2-((4-Methoxyphenyl)amino)ethyl)-1,3,5-Triazine-2,4,6-Triamine Hydrochloride (**15**)

White solid (60% yield), mp: 150–153 °C; ¹H NMR (600 MHz, MeOD) δ 7.59 (d, J = 7.6 Hz, 1H), 7.54–7.44 (m, 2H), 7.40–7.35 (m, 2H), 7.11 (t, J = 6.0 Hz, 2H), 7.03 (dd, J = 19.2, 7.7 Hz, 1H), 6.97 (d, J = 8.9 Hz, 1H), 3.83 (d, J = 13.4 Hz, 2H), 3.75 (s, 3H), 3.71 (t, J = 7.0 Hz, 1H), 3.65 (t, J = 5.6 Hz, 1H), 3.60 (t, J = 5.7 Hz, 1H), 3.56 (t, J = 5.7 Hz, 1H), 3.09 (t, J = 6.6 Hz, 1H), 3.04 (t, J = 6.9 Hz, 1H); ¹³C NMR (151 MHz, MeOD) δ 160.4, 156.2, 136.8, 127.4, 127.3, 127.0, 123.6, 122.4, 121.0, 118.3, 117.7, 115.1, 111.2, 111.0, 110.9, 54.8, 41.35, 36.7, 36.3, 24.8; HPLC-MS analysis t–5.20 min (100% purity, method A), calc. for C₂₂H₂₆N₈O *m/z* = 418.2, found *m/z* = 419.2 [M+H]⁺

4.1.27. Synthesis of Tert-Butyl-(2-Chloroethyl)Carbamate (**70**)

To a suspension of 2-chloroethanamine hydrochloride **52** (5 g, 43.1 mmol) in 60 mL DCM cooled to 0 °C, triethylamine (12 mL, 86.1 mmol) was added, followed by di-tert-butyl decarbonate (11.2 g, 51.4 mmol). The reaction was carried out at room temperature for 12 h. After this period reaction mixture was washed three times with 0.1M HCl and water. Organic layers were combined, dried over MgSO₄ then evaporated to dryness, yielding colorless sticky oil **70**.

4.1.28. General Procedure for the Synthesis of **75–78** (Microwave-Assisted)

Starting material **71–74** (3.7 mmol), tert-butyl-(2-chloroethyl)carbamate **70** (5.6 mmol), sodium hydroxide (5.6 mmol), and TBAB (0.4 mmol) were ground in a mortar and transferred to a sealed tube. Subsequently, 5 wt % DMF was added. The mixture was reacted in a microwave reactor at 65 W for 60 s. Reaction progress was monitored via TLC (chloroform: MeOH 9:1, *v/v*). The mixture was extracted with chloroform (3 × 30 mL), organic layers were combined, dried over MgSO₄ then evaporated to dryness. The crude product was purified via column chromatography, eluting with chloroform then chloroform:MeOH (*v/v*) 99:1 → 97:3. Obtained pale yellow solid was then dissolved in 30 mL DCM followed by the addition of 4M HCl in 1,4-dioxane to reach pH = 2. The mixture was stirred at room temperature for 12 h, and then the solid was filtered, washed with DCM and diethyl ether, and dried, yielding titled compounds **75–78**.

4.1.29. General Procedure for the Synthesis of Final Compounds **16–19** (Microwave-Assisted)

Briefly, **69** [20] (0.25 g, 0.8 mmol), amine hydrochloride **75–78** (2.0 mmol), potassium carbonate (0.36 g, 2.5 mmol) and TBAB (0.032 g, 0.1 mmol) were ground in a mortar and transferred to a sealed tube. Subsequently, 5 wt % DMF was added. The mixture was reacted in a microwave reactor at 50 W for 2.5 min. Reaction progress was monitored via TLC (chloroform: MeOH 9:1 *v/v*). The mixture was cooled down and extracted with chloroform (3 × 20 mL). Organic layers were combined, dried over MgSO₄, and concentrated. The crude product was purified via column chromatography with elution using chloroform then chloroform:MeOH (*v/v*) 99:1 → 88:12. Beige sticky oil was then dissolved in acetone, and pH was adjusted to 2–3 with 4 M HCl in 1,4-dioxane. The resulting mixture was crushed by the addition of cold diethyl ether, and then the beige powder was filtered and rinsed with cold diethyl ether and then dried to yield final product **16–19**.

4.1.30. 2-(2-((4-((2-(1H-Indol-3-yl)ethyl)amino)-6-Amino-1,3,5-Triazin-2-yl)amino)ethyl)is-oidoline-1,3-Dione Hydrochloride (**16**)

White solid (59% yield), mp: 136–138 °C; ¹H NMR (600 MHz, MeOD) δ 7.87–7.66 (m, 4H), 7.56 (d, J = 7.9 Hz, 1H), 7.34 (dd, J = 14.8, 7.9 Hz, 1H), 7.14–6.95 (m, 3H), 3.91 (bs, 1H), 3.84 (t, J = 5.1 Hz, 1H), 3.69–3.50 (m, 4H), 3.07–2.88 (m, 2H); ¹³C NMR (151 MHz, MeOD) δ 168.5, 168.3, 136.7, 133.9, 131.9, 127.3, 122.7, 122.4, 121.0, 120.9, 118.3, 118.1, 117.8, 111.4, 110.8, 41.1, 38.7, 36.9, 24.9; HPLC-MS analysis t–5.41 min (100% purity, method A), calc. for C₂₃H₂₂N₈O₂ *m/z* = 442.2, found *m/z* = 443.2 [M+H]⁺.

4.1.31. N²-(2-(1H-Benzo[d]imidazol-1-yl)ethyl)-N⁴-(2-(1H-Indol-3-yl)ethyl)-1,3,5-Triazine-2,4,6-Triamine Hydrochloride (17)

White solid (60% yield), mp: 195–200 °C; ¹H NMR (600 MHz, MeOD) δ 9.44 (s, 1H)–hydrogen bonded rotamer H-N_{benzimid.}, 8.00–7.84 (m, 1H), 7.80 (dd, J = 21.4, 8.3 Hz, 1H), 7.70–7.45 (m, 3H), 7.34 (dd, J = 32.3, 7.9 Hz, 1H), 7.14–7.00 (m, 3H), 4.80 (t, J = 5.4 Hz, 1H), 4.55 (t, J = 5.4 Hz, 1H), 3.97 (t, J = 4.9 Hz, 1H), 3.68 (dd, J = 19.7, 4.9 Hz, 2H), 3.24 (t, J = 6.9 Hz, 1H), 3.03 (dd, J = 15.5, 7.9 Hz, 1H), 2.90 (t, J = 6.8 Hz, 1H); ¹³C NMR (151 MHz, MeOD) δ 156.1, 140.7, 136.7, 130.7, 127.2, 126.9, 126.5, 122.5, 121.0, 118.2, 117.7, 114.3, 112.5, 111.2, 111.0, 46.3, 40.9, 39.4, 24.8; HPLC-MS analysis t–4.76 min (96% purity, method A), calc. for C₂₂H₂₃N₉ m/z = 413.2, found m/z = 414.2 [M+H]⁺.

4.1.32. N²-(2-(1H-indol-3-yl)ethyl)-N⁴-(2-(2-methyl-1H-benzo[d]imidazol-1-yl)ethyl)-1,3,5-triazine-2,4,6-triamine hydrochloride (18)

White solid (55% yield), mp: 190–194 °C; ¹H NMR (600 MHz, MeOD) δ 7.73–7.63 (m, 1H), 7.63–7.48 (m, 3H), 7.41–7.29 (m, 2H), 7.12 (dd, J = 14.4, 7.8 Hz, 1H), 7.09–7.00 (m, 2H), 4.69 (bs, 1H), 4.44 (t, J = 5.5 Hz, 1H), 3.93 (t, J = 5.1 Hz, 1H), 3.69 (t, J = 4.8 Hz, 1H), 3.62 (t, J = 7.0 Hz, 1H), 3.30 (t, J = 6.9 Hz, 1H), 3.14–2.97 (m, 4H), 2.75 (s, 1H); ¹³C NMR (151 MHz, MeOD) δ 156.1, 150.9, 136.7, 132.0, 127.3, 126.3, 125.9, 122.6, 121.0, 118.3, 117.9, 113.3, 112.1, 111.2, 111.0, 44.3, 41.0, 38.9, 24.7, 10.3; HPLC-MS analysis t–4.25 min (97% purity, method A), calc. for C₂₃H₂₅N₉ m/z = 427.2, found m/z = 428.2 [M+H]⁺.

4.1.33. N²-(2-(1H-Indol-3-yl)ethyl)-N⁴-(2-(2-(Trifluoromethyl)-1H-Benzo[d]imidazol-1-yl)ethyl)-1,3,5-Triazine-2,4,6-Triamine Hydrochloride (19)

White solid (76% yield), mp: 108–110 °C; ¹H NMR (600 MHz, MeOD) δ 8.15–7.72 (m, 2H), 7.61–7.47 (m, 2H), 7.44 (d, J = 7.7 Hz, 1H), 7.35 (d, J = 8.0 Hz, 1H), 7.11 (dd, J = 24.3, 17.3 Hz, 2H), 7.06–6.95 (m, 1H), 3.77 (dt, J = 47.9, 6.7 Hz, 2H), 3.11 (t, J = 6.3 Hz, 2H); ¹³C NMR (151 MHz, DMSO) δ 156.1, 140.8, 136.7, 136.0, 127.5, 125.6, 123.9, 123.3, 121.2, 120.4, 118.6, 118.5, 112.1, 111.8, 111.4, 44.7, 41.1, 30.0, 27.5, 24.9; HPLC-MS analysis t–5.85 min (92 % purity, method A), calc. for C₂₃H₂₂F₃N₉ m/z = 481.2, found m/z = 482.2 [M+H]⁺.

4.1.34. General Procedure for the Synthesis of Final Compounds 20–22 (Microwave-Assisted)

Briefly, **69** [20] (0.25 g, 0.8 mmol), amines **62**, **66**, and **68** (2.0 mmol) potassium carbonate (0.36 g, 2.5 mmol) and TBAB (0.032 g, 0.1 mmol) were ground in a mortar and transferred to a sealed tube. Subsequently, 5 wt % DMF was added. The mixture was reacted in a microwave reactor at 50 W for 2.5 min. Reaction progress was monitored via TLC (chloroform: MeOH 9:1 v/v). The mixture was cooled down and extracted with chloroform (3 × 20 mL). Organic layers were combined, dried over MgSO₄, and concentrated. The crude product was purified via column chromatography with elution using chloroform then chloroform:MeOH (v/v) 99:1-> 97:3. Colorless sticky oil was then dissolved in acetone, and pH was adjusted to 2–3 with 4 M HCl in 1,4-dioxane. The resulting mixture was crushed by the addition of cold diethyl ether, then the white powder was filtered and rinsed with cold diethyl ether and then dried to yield the final product **20–22**.

4.1.35. N²-(2-(1H-Indol-3-yl)ethyl)-N⁴-(3-Chlorophenyl)-1,3,5-Triazine-2,4,6-Triamine Hydrochloride (20)

White solid (84% yield), mp: 174–178 °C; ¹H NMR (600 MHz, MeOD) δ 7.80 (d, J = 20.9 Hz, 1H), 7.63–7.42 (m, 2H), 7.38–7.27 (m, 2H), 7.20–7.08 (m, 3H), 7.06–6.98 (m, 1H), 3.84–3.70 (m, 2H), 3.11 (t, J = 7.0 Hz, 2H); ¹³C NMR (151 MHz, MeOD) δ 136.8, 133.9, 129.6, 127.2, 124.0, 122.4, 121.2, 121.0, 119.5, 118.3, 117.7, 111.0, 110.9, 41.6, 24.5; HPLC-MS analysis t–6.53 min (100% purity, method A), calc. for C₁₉H₁₈³⁵ClN₇ m/z = 379.1, found m/z = 380.1 [M+H]⁺, calc. for C₁₉H₁₈³⁷ClN₇ m/z = 381.1, found m/z = 382.1 [M+H]⁺.

4.1.36. N²-(2-(1H-Indol-3-yl)ethyl)-N⁴-(4-Fluorophenyl)-1,3,5-Triazine-2,4,6-Triamine Hydrochloride (**21**)

White solid (82% yield), mp: 232–235 °C; ¹H NMR (600 MHz, MeOD) δ 7.69–7.46 (m, 3H), 7.36 (d, J = 8.1 Hz, 1H), 7.16–6.99 (m, 5H), 3.75 (bs, 2H), 3.09 (bs, 2H); ¹³C NMR (151 MHz, MeOD) δ 136.8, 127.2, 123.8, 122.3, 121.0, 118.3, 117.7, 115.0, 114.8, 111.2, 110.9, 41.4, 24.6; HPLC-MS analysis t–5.97 min (100% purity, method A), calc. for C₁₉H₁₈FN₇ m/z = 363.2, found m/z = 364.4 [M+H]⁺.

4.1.37. N²-(2-(1H-Indol-3-yl)ethyl)-N⁴-(4-Methoxyphenyl)-1,3,5-Triazine-2,4,6-Triamine Hydrochloride (**22**)

White solid (83% yield), mp: 194–196 °C; ¹H NMR (600 MHz, MeOD) δ 7.61–7.38 (m, 3H), 7.36 (d, J = 8.1 Hz, 1H), 7.15–7.08 (m, 2H), 7.06–6.91 (m, 2H), 6.84 (bs, 1H), 3.84–3.67 (m, 5H), 3.07 (bs, 2H); ¹³C NMR (151 MHz, MeOD) δ 136.8, 127.2, 123.5, 122.3, 121.0, 118.3, 117.8, 114.1, 113.6, 111.2, 110.9, 54.5, 41.4, 24.6; HPLC-MS analysis t–5.88 min (100% purity, method A), calc. for C₂₀H₂₁N₇O m/z = 375.2, found m/z = 376.1 [M+H]⁺.

4.2. Radioligand Assay

The cell culture, cell membranes, and radioligand binding assays were performed in accordance with standard protocols [17].

4.3. Atlas Activity

Activity maps were prepared using the Atlas Activity tool available in Flare [24] according to the procedure described in a previous paper [15].

4.4. Molecular Modelling

A homologous model developed by us earlier was used for molecular modeling studies [15]. The docking procedure and the QM–MM optimization of the ligand–receptor complex were performed according to a previously described protocol [15,20,32].

4.5. Metabolic Stability

All assays were performed according to the protocols described previously [15,33–35].

4.6. CYP3A4 Activity

All assays were performed according to the protocols described previously [15,33–35].

4.7. Hepatotoxicity

All assays were performed according to the protocols described previously [15,33–35].

4.8. In Vivo Cardiotoxicity

To determine the toxicity of the compounds, the fish embryo toxicity (FET) test was performed on zebrafish (*Danio rerio*) according to OECD Test Guideline 236. The collected embryos were transferred to a Petri dish with E3 medium (5 mM NaCl, 0.33 mM MgCl₂, 0.33 mM CaCl₂, 0.17 mM KCl; pH 7.2) and then placed in 6-well plates, 10 embryos per well. Stock solutions **2** and **12** were prepared in DMSO. In these experiments, the range of different concentrations of the solutions was prepared by dissolving stock solutions in the E3 medium each time directly before addition to the wells. The solutions were changed once daily, and the embryos were maintained in the incubator at 28.5 °C. At the end of the exposure period (96 hpf–hours postfertilization), acute toxicity was determined based on a positive outcome in any of the four visual indicators of lethality, including the coagulation of fertilized eggs, lack of somite formation, lack of detachment of the tailbud from the yolk sac and lack of heartbeat. The value of LD₅₀ was calculated. Heartbeats were recorded to observe cardiotoxic effects. Moreover, images of the fish from each group were taken at the final time point to monitor the occurrence of developmental malformations. For the observations, a Discovery V8 Stereo optical microscope and Zeiss hardware were used.

A dose-response curve was generated using Prism 8.0.1 (GraphPad Software) by fitting a sigmoid curve model to experimental data points. The concentrations of the compounds of interest causing 50% mortality (LD₅₀) of 96 hpf larvae of *Danio rerio* were calculated.

Supplementary Materials: The following supporting information can be downloaded at: <https://www.mdpi.com/article/10.3390/ijms232113308/s1>, Copies of the ¹H and ¹³C NMR spectra and HPLC-MS analysis, metabolic stability-MS spectrograms and 5-HT₇ receptor homology model validation can be found in the Supplementary Material.

Author Contributions: Conceptualization, D.K.; methodology, D.K.; software, D.K. and G.L.; validation, D.K.; formal analysis, D.K. and D.P.; investigation, D.K., A.K.D., G.S., G.L., D.P. and A.B.-C.; writing—original draft preparation, D.K.; writing—review and editing, D.K., D.P. and J.J.; visualization, D.K.; supervision, D.K.; project administration, D.K.; funding acquisition, D.K. All authors have read and agreed to the published version of the manuscript.

Funding: This research was funded by National Center for Research and Development (project No. LID-ER/41/0206/L-12/20/NCBR/2021) and PL-Grid infrastructure (Prometheus, ACCCYFRONET, AGH, project ID: drugdesign5).

Institutional Review Board Statement: Not applicable.

Informed Consent Statement: Not applicable.

Data Availability Statement: Not applicable.

Conflicts of Interest: The authors declare no conflict of interest.

References

1. Vanhoenacker, P.; Haegeman, G.; Leysen, J.E. 5-HT₇ receptors: Current knowledge and future prospects. *Trends Pharmacol. Sci.* **2000**, *21*, 70–77. [[CrossRef](#)]
2. Naumenko, V.S.; Popova, N.K.; Lacivita, E.; Leopoldo, M.; Ponimaskin, E.G. Interplay between serotonin 5-HT_{1A} and 5-HT₇ receptors in depressive disorders. *CNS Neurosci. Ther.* **2014**, *20*, 582–590. [[CrossRef](#)] [[PubMed](#)]
3. Hauser, S.R.; Hedlund, P.B.; Roberts, A.J.; Sari, Y.; Bell, R.L.; Engleman, E.A. The 5-HT₇ receptor as a potential target for treating drug and alcohol abuse. *Front. Neurosci.* **2015**, *8*, 448. [[CrossRef](#)] [[PubMed](#)]
4. Kim, J.J.; Khan, W.I. 5-HT₇ receptor signaling: Improved therapeutic strategy in gut disorders. *Front. Behav. Neurosci.* **2014**, *8*, 396. [[CrossRef](#)]
5. Stull, M.A.; Pai, V.; Vomachka, A.J.; Marshall, A.M.; Jacob, G.A.; Horseman, N.D. Mammary gland homeostasis employs serotonergic regulation of epithelial tight junctions. *Proc. Natl. Acad. Sci. USA* **2007**, *104*, 16708–16713. [[CrossRef](#)]
6. Cadirci, E.; Halici, Z.; Bayir, Y.; Albayrak, A.; Karakus, E.; Polat, B.; Unal, D.; Atamanalp, S.S.; Aksak, S.; Gundogdu, C. Peripheral 5-HT₇ receptors as a new target for prevention of lung injury and mortality in septic rats. *Immunobiology* **2013**, *218*, 1271–1283. [[CrossRef](#)]
7. Cinar, I.; Sirin, B.; Halici, Z.; Palabiyik-Yucelik, S.S.; Akpınar, E.; Cadirci, E. 5-HT₇ receptors as a new target for prostate cancer pathophysiology and treatment: An experimental study on PC-3 cells and FFPE tissues. *Naunyn-Schmiedeberg's Arch. Pharmacol.* **2021**, *394*, 1205–1213. [[CrossRef](#)] [[PubMed](#)]
8. Modica, M.N.; Lacivita, E.; Intagliata, S.; Salerno, L.; Romeo, G.; Pittalà, V.; Leopoldo, M. Structure-Activity Relationships and Therapeutic Potentials of 5-HT₇ Receptor Ligands: An Update. *J. Med. Chem.* **2018**, *61*, 8475–8503. [[CrossRef](#)]
9. Guseva, D.; Wirth, A.; Ponimaskin, E. Cellular mechanisms of the 5-HT₇ receptor-mediated signaling. *Front. Behav. Neurosci.* **2014**, *8*, 306. [[CrossRef](#)]
10. Ye, D.; Xu, H.; Tang, Q.; Xia, H.; Zhang, C.; Bi, F. The role of 5-HT metabolism in cancer. *Biochim. Biophys. Acta. Rev. Cancer* **2021**, *1876*, 188618. [[CrossRef](#)]
11. Gautam, J.; Banskota, S.; Regmi, S.C.; Ahn, S.; Jeon, Y.H.; Jeong, H.; Kim, S.J.; Nam, T.G.; Jeong, B.S.; Kim, A.J. Tryptophan hydroxylase 1 and 5-HT₇ receptor preferentially expressed in triple-negative breast cancer promote cancer progression through autocrine serotonin signaling. *Mol. Cancer* **2016**, *15*, 75. [[CrossRef](#)] [[PubMed](#)]
12. Du, X.; Wang, T.; Wang, Z.; Wu, X.; Gu, Y.; Huang, Q.; Wang, J.; Xie, J. 5-HT₇ Receptor Contributes to Proliferation, Migration and Invasion in NSCLC Cells. *Onco Targets Ther.* **2020**, *13*, 2139–2151. [[CrossRef](#)] [[PubMed](#)]
13. Quintero-Villegas, A.; Valdés-Ferrer, S.I. Role of 5-HT₇ receptors in the immune system in health and disease. *Mol. Med.* **2020**, *26*, 2. [[CrossRef](#)] [[PubMed](#)]
14. Albayrak, A.; Halici, Z.; Cadirci, E.; Polat, B.; Karakus, E.; Bayir, Y.; Unal, D.; Atasoy, M.; Dogrul, A. Inflammation and peripheral 5-HT₇ receptors: The role of 5-HT₇ receptors in carrageenan induced inflammation in rats. *Eur. J. Pharmacol.* **2013**, *715*, 270–279. [[CrossRef](#)] [[PubMed](#)]

15. Kułaga, D.; Drabczyk, A.K.; Satała, G.; Latacz, G.; Rózga, K.; Plażuk, D.; Jaśkowska, J. Design and synthesis of new potent 5-HT₇ receptor ligands as a candidate for the treatment of central nervous system diseases. *Eur. J. Med. Chem.* **2022**, *227*, 113931. [[CrossRef](#)]
16. Vermeulen, E.S.; Schmidt, A.W.; Sprouse, J.S.; Wikström, H.V.; Grol, C.J. Characterization of the 5-HT₇ receptor. Determination of the pharmacophore for 5-HT₇ receptor agonism and CoMFA-based modeling of the agonist binding site. *J. Med. Chem.* **2003**, *46*, 5365–5374. [[CrossRef](#)]
17. Hogendorf, A.S.; Hogendorf, A.; Kurczab, R.; Satała, G.; Lenda, T.; Walczak, M.; Latacz, G.; Handzlik, J.; Kieć-Kononowicz, K.; Wierońska, J.M.; et al. Low-basicity 5-HT₇ Receptor Agonists Synthesized Using the van Leusen Multicomponent Protocol. *Sci. Rep.* **2017**, *7*, 1444. [[CrossRef](#)]
18. Gillis, E.P.; Eastman, K.J.; Hill, M.D.; Donnelly, D.J.; Meanwell, N.A. Applications of Fluorine in Medicinal Chemistry. *J. Med. Chem.* **2015**, *58*, 8315–8359. [[CrossRef](#)]
19. Smith, D.A. *Metabolism, Pharmacokinetics and Toxicity of Functional Groups: Impact of Chemical Building Blocks on ADMET*; Drug Discovery; The Royal Society of Chemistry: London, UK, 2010; Chapter 2; pp. 61–98.
20. Kułaga, D.; Jaśkowska, J.; Satała, G.; Latacz, G.; Śliwa, P. Aminotriazines with indole motif as novel, 5-HT₇ receptor ligands with atypical binding mode. *Bioorg. Chem.* **2020**, *104*, 104254. [[CrossRef](#)]
21. Mattson, R.J.; Denhart, D.J.; Catt, J.D.; Dee, M.F.; Deskus, J.A.; Ditta, J.L.; Epperson, J.; Dalton King, H.; Gao, A.; Poss, M.A.; et al. Aminotriazine 5-HT₇ antagonists. *Bioorg. Med. Chem. Lett.* **2004**, *14*, 4245–4248. [[CrossRef](#)]
22. Chen, Z.; Cohen, M.P.; Fisher, M.J.; Gillig, J.R.; McCowan, J.R.; Miller, S.C.; Schaus, J.M.; Giethlen, B. N-(2-arylethyl) Benzylamines as Antagonists of the 5-HT₆ Receptor. EP1859798A1, 28 November 2007.
23. Cheng, Y.; Prusoff, W.H. Relationship between the inhibition constant (K_i) and the concentration of inhibitor which causes 50 per cent inhibition (IC_{50}) of an enzymatic reaction. *Biochem. Pharmacol.* **1973**, *22*, 3099–3108. [[PubMed](#)]
24. Flare, version 5, Cresset®, Litlington, Cambridgeshire, UK. Available online: <http://www.cresset-group.com/flare> (accessed on 2 May 2022).
25. *Schrödinger Release 2016-4: Maestro*; Schrödinger; LLC: New York, NY, USA, 2016.
26. Impellizzeri, A.A.R.; Pappalardo Basile, M.L.; Manfra, O.; Andressen, K.W.; Krobert, K.A.; Messina, A.; Levy, F.O.; Guccione, S. Identification of essential residues for binding and activation in the human 5-HT_{7(a)} serotonin receptor by molecular modeling and site-directed mutagenesis. *Front. Behav. Neurosci.* **2015**, *9*, 92. [[CrossRef](#)] [[PubMed](#)]
27. Wichur, T.; Godyń, J.; Góral, I.; Latacz, G.; Bucki, A.; Siwek, A.; Głuch-Lutwin, M.; Mordyl, B.; Śniecikowska, J.; Walczak, M.; et al. Development and crystallography-aided SAR studies of multifunctional BuChE inhibitors and 5-HT₆ R antagonists with β -amyloid anti-aggregation properties. *Eur. J. Med. Chem.* **2021**, *225*, 113792. [[CrossRef](#)] [[PubMed](#)]
28. Luo, G.; Guenther, T.; Gan, L.; Humphreys, W.G. CYP3A4 Induction by Xenobiotics: Biochemistry, Experimental Methods and Impact on Drug Discovery and Development. *Curr. Drug Metab.* **2004**, *5*, 483–505. [[CrossRef](#)]
29. OECD. *Test No. 236: Fish Embryo Acute Toxicity (FET) Test, OECD Guidelines for the Testing of Chemicals; Section 2*; OECD Publishing: Paris, France, 2013. [[CrossRef](#)]
30. Hedlund, P.B. The 5-HT₇ receptor and disorders of the nervous system: An overview. *Psychopharmacol.* **2009**, *206*, 345–354. [[CrossRef](#)]
31. Gregory, A.W.; Jakubec, P.; Turner, P.; Dixon, D.J. Gold and BINOL-Phosphoric Acid Catalyzed Enantioselective Hydroamination/N-Sulfonyliminium Cyclization Cascade. *Org. Lett.* **2013**, *15*, 4330–4333. [[CrossRef](#)]
32. Kułaga, D.; Jaśkowska, J.; Satała, G. Design, synthesis and biological evaluation of novel serotonin and dopamine receptor ligands being 6-bromohexyl saccharine derivatives, *Bioorg. Med. Chem. Lett.* **2019**, *29*, 126667. [[CrossRef](#)]
33. Latacz, G.; Hogendorf, G.A.S.; Hogendorf, A.; Lubelska, A.; Wieronska, J.M.; Wozniak, M.; Cieslik, P.; Kieć-Kononowicz, K.; Handzlik, J.; Bojarski, A.J. Search for a 5-CT alternative. In vitro and in vivo evaluation of novel pharmacological tools: 3-(1-alkyl-1H-imidazol-5-yl)-1H-indole-5-carboxamides, low-basicity 5-HT₇ receptor agonists. *Med. Chem. Comm.* **2018**, *9*, 1882–1890. [[CrossRef](#)]
34. Latacz, G.; Lubelska, A.; Jastrzebska-Wiesek, M.; Partyka, A.; Kucwaj-Brysz, K.; Wesółowska, A.; Kieć Kononowicz, K.; Handzlik, J. MF-8, a novel promising arylpiperazine-hydantoin based 5-HT₇ receptor antagonist: In vitro drug-likeness studies and in vivo pharmacological evaluation. *Bioorg. Med. Chem. Lett.* **2018**, *28*, 878–883. [[CrossRef](#)]
35. Latacz, G.; Lubelska, A.; Jastrzebska-Więsek, M.; Partyka, A.; Sobilo, A.; Olejarz, A.; Kucwaj-Brysz, K.; Satała, G.; Bojarski, A.J.; Wesółowska, A.; et al. In the search for a lead structure among series of potent and selective hydantoin 5-HT₇R agents: The drug-likeness in vitro study. *Chem. Biol. Drug Des.* **2017**, *90*, 1295–1306. [[CrossRef](#)]